Doctoral Dissertation

Studies on Fabrication of Fully Single-charged Layer-by-layer Nanofilms by Stepwise Crosslinking

ZHANG ZHUYING

July 2024

Graduate School of Engineering

Osaka University

Content

General Introduction

The methods of surface modifications are important in generating materials with functional surface (**Figure 1**). By adjusting the surface functionalization, surface grafting, surface topography modification, and coating on the surface, the properties of surface can be modified while preserving the underlying structures. Among all the surface modification methods, coating has the highest cost-benefit ratio of the material used[1]. So coating is an economic method for surface modification.

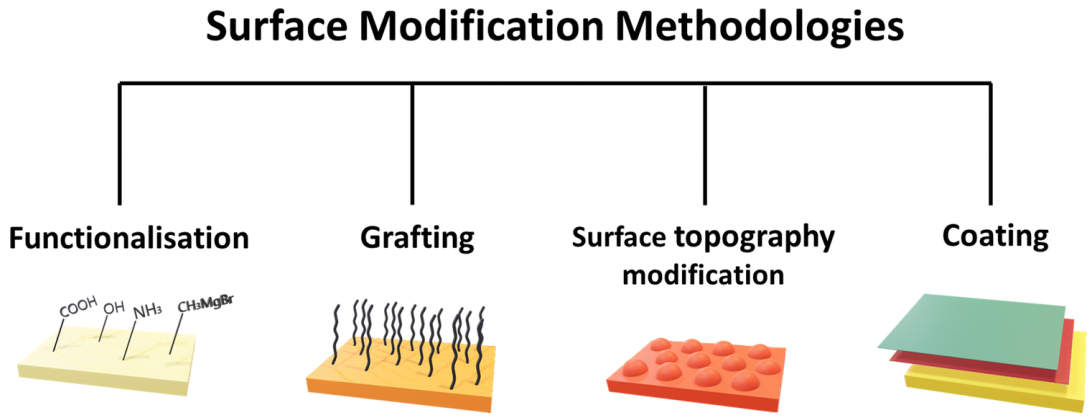

Figure 1 Schematic illustration of surface modification methods[1]

Layer-by-layer (LbL) assembly is a popular and attractive technique to functionalize the surface in a simple, controllable manner. Generally, LbL assembly involves the cyclical deposition of different materials onto substrates, leading to the gradual growth of thin films. The main advantage of this technique is the ability to create stable deposited nanoscale thin films with well-organized structures and tunable composition on different substrates.[2–4] This technology can be traced back to the 1960s when Iler[5] and Kirkland[6] fabricated inorganic films by assembling positively-charged alumina fibers and negatively-charged silica particles. The LbL assembly technique has since experienced a period of explosive growth, being widely used as a versatile, simple, convenient strategy to fabricate multilayer materials with tunable structures, composition, and physicochemical properties.

LbL Assembly technologies can currently be classified into five main categories: 1) dip assembly, 2) spin-assisted assembly, 3) spray assembly, 4) microfluidic systems and 5) 3D printing. Of these five major assembly technologies, dipping assembly has been researched

the longest, while microfluidic systems and 3D printing have been developed more recently. Dip assembly is the most common LbL assembly method, involving the alternate adsorption of two or more different desired material solutions, with intermediate washing steps.[7,8] It is usually performed by manually immersing a substrate into a solution of the desired materials to modify the surface function.

The film properties are influenced by solution properties such as concentration and charge density, as well as process parameters such as dip time and rinse time.[9] Specifically, a higher concentration increases the quantity of adsorbed materials, leading to a thicker nanofilm. High concentration can also increase the viscosity of the solution, slowing the rate of material diffusion and prolonging the time for the films to reach equilibrium. It should be noted that when solution concentration is below a certain level, interdigitation between the layers occurs as a result of interdiffusion. However, cell adhesion is enhanced on the interdigitation layers as the result of increased stiffness.[10] The dipping time for the adsorption of each layer is of crucial importance. A short dipping time results in kinetically trapped polymers,[11] while a longer dipping time allows for adequate layer deposition and polymer chain rearrangement. However, a much longer dipping time can weaken the stratified structures of the films.[12] Dip LbL assembly on different substrates[13] has a variety of potential applications.

I. Regulate cell behavior

Cell behavior on LbL assembly films can be regulated by stiffness, morphology, biological properties, and release properties of films.[14] The chemical properties of multilayers are highly dependent on their composition. For example, cell adhesion is promoted by the use of materials that are known to have adhesive properties. Arginine-glycine-aspartic acid (RGD) [15–17] and catechol groups,[18,19] either acting as an assembly component or as a partial structure of the polymers, have been used to support cell and protein adhesion due to the enriched interactions between surfaces and cells. For the control of other cell behaviors like proliferation and differentiation, more complex structures and accurate adjustment of surface properties are required. Chitosan/fibrinogen multilayers have been fabricated for improving the adhesion and spreading of cardiomyocytes.[20] It was reported that a pure fibrinogen coating was sufficient for cell adhesion and spreading, but chitosan tuned the absorbed fibrinogen amount, facilitating the identification of the optimal surface properties for cell proliferation.

II. Controlled drug-releasing properties

The releasing properties of a film are usually achieved by stimuli-responsive residues. For LbL films, electrostatic interactions, hydrogen bonds, and host-guest interactions are generally non-covalent interactions and a drastic change in the external environment, such as pH and temperature, will result in the dissociation of multilayer films in an aqueous solution. This dissociation can be exploited to create responsive burst release systems.[21]

When two or more types of interactions are induced, it is possible to break just one kind of interaction and retain the other. Based on this, a reusable platform for protein and bacterial capture and release was developed.[22] The platform was assembled via host-guest interactions and electrostatic interactions. Because of the inherent reversibility of host-guest interactions, the paired structure was dissociated by incubating with sodium dodecyl sulfate without destroying the structure of the multilayered film, allowing the captured proteins and bacteria to be released from the platform and then renewing the "guest" surface for the next capture of proteins and bacteria.

To improve the stability of the assembled film for wider application, the electrostatic interaction and hydrogen bond can be further crosslinked to form covalent bonds in physiological conditions. Different crosslinking methods (photo crosslinking,[23] thermal crosslinking[24]) can be chosen based on the chemical properties of film components. After partial crosslinking, there are both stable and reversible interactions that enable the film to respond to stimuli while maintaining the LbL structure, allowing for controlled release.[25]

III. Cell encapsulation

Encapsulating living cells has garnered considerable interest in biomedical fields, like transplantation therapy, tissue engineering, and cell-based biosensors. Numerous reviews have focused on the materials,[26] strategies,[27,28] and applications,[29–31] of cell encapsulation. Briefly, a variety of materials have been used for LbL cell encapsulation including polysaccharides, proteins, and even nanoparticles.[32,33] Living cells are more sensitive to their surroundings so the encapsulation process must be performed under physiological conditions to maintain cell viability.[34]

Cell encapsulation enables attenuation of the host immunological response in cell transplantation,[35] incorporation of functional molecules to regulate cell biological behavior,

and modification of the cells' surface to endow them with new features for tissue engineering,[36] etc. Our group has successfully constructed extracellular matrix (ECM)-like films on a cell surface with the layer-by-layer assembly of fibronectin (FN) and gelatin (G). The FN/G film acted as an ECM-like support,[37] protecting the cells from contact inhibition and promoting cell-cell adhesions.[38] This technology will be promising for the engineering of 3D tissue.

Dip assembly is the simplest and most widely used LbL method. The properties of films fabricated by this method are mostly related to the material properties. Dip time and rinsing time are the only two process parameters that affect the film's properties. The film stiffness and internal structure can be adjusted to suit cell adhesion and drug loading.

Many years of development in both the driving forces have seen the current research field of LbL greatly exceed that of Decher's era. The driving forces mostly related to the materials used, the choice of which are highly dependent on their intrinsic properties for desired functions. As well as polyelectrolytes, other materials like synthetic polymers,[39] proteins,[40] nucleic acids,[41] and nanoparticles[42] are also used as building blocks, provided they can interact with each other. The diversity of materials has enriched the interactions of multilayers. Hydrogen bond, host-guest interaction, hydrophobic interaction, and covalent bond are frequently used to drive LbL assembly. Polyelectrolyte LbL assembly films based on electrostatic interactions are still the most investigated as they allow for the quick construction of materials with multiple functionalities. So polyelectrolytes (PE) become the first choice for LbL nanofilm fabrication. However, it was not until the 1990s that Decher fabricated multilayer films by consecutive adsorption of polyanions and polycations (**Figure 2**), a more versatile technique that relies on solutions of macromolecules and could thus be successfully extended to other materials.[43,44] The wide range of materials make it possible for the fabricated PE nanofilms to be applied in many fields, like regulating the cell environment[37] and surface modification[45] for different functions. Pichart's group[46] used poly(L-lysine)/hyaluronan (PLL/HA) LbL films loaded with bone morphogenetic protein 2 (BMP-2) to promote differentiation from myoblasts to osteoblasts. Chen[22] fabricated a platform coated with poly(allylamine hydrochloride) (PAH)/poly(acrylic acid-co-1-adamantan-1-ylmethyl acrylate) (P(AA-co-Ada)) LbL film for the capture of proteins and bacteria.

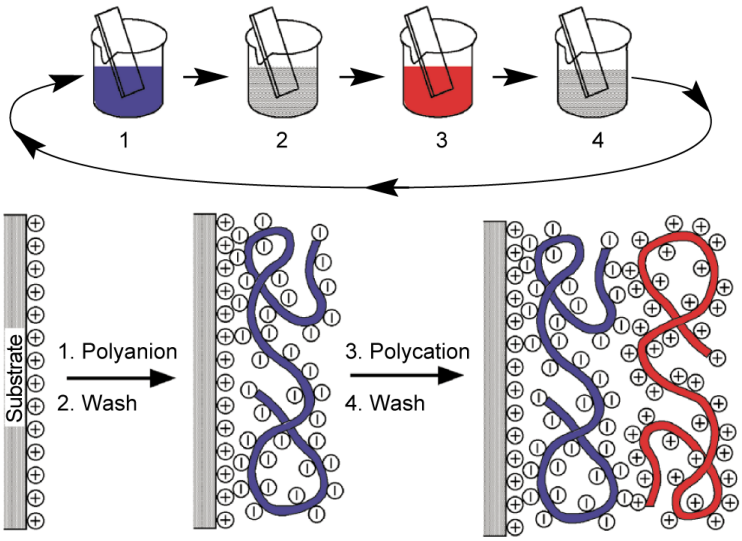

Figure 2 Schematic illustration of the PE LbL assembly process and (b) the alternate deposition of polyanion and polycation on the substrate for films construction.[44]

However, there still remains some limitations of PE LbL nanofilms. As shown in **Figure 3a**, when comes to the ion permeation, due to their multi-bipolar architecture, the films would reject ions by electrostatic repulsions. It also been demonstrated that divalent ions receive a much stronger repulsion than monovalent ions.[47] It is shown that the ion permeation depends on the concentration of excess charges, which can be different upon varied conditions of film preparation.

The limitation in ion permeation further affects the adsorption properties of PE LbL nanofilms. As shown in **Figure 3b**, when adsorbing the charged bioactive molecules, the molecules aggregate on the surface of the nanofilms but find it difficult to penetrate inside the films. Salloum and Schleoff[48] proved that the surface charge of PE films affect the adsorption behaviour of charged molecules. When using PE nanofilms fabricated by Poly(N-methyl-2-vinyl pyridinium bromide (PM2VP) and Poly(styrenesulfonic acid) (PSS) to absorb the negative charged BSA, the PE films with positive charged surface exhibit a higher loading amount compared to the same PE films but with the negative charged surface.

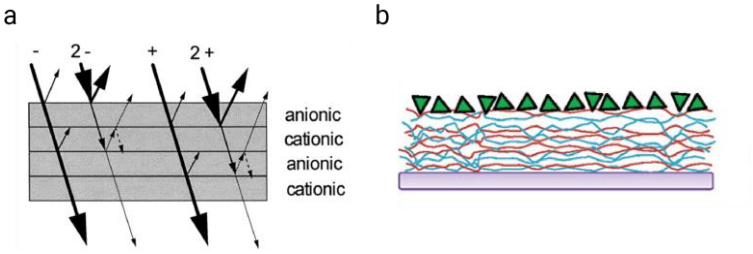

Figure 3 (a) Ion rejection model of polyelectrolyte films.[49] (b) Aggregation of bioactive molecules during the adsorption by PE films.[50]

In addition, because of the assembly mechanism of PE LbL nanofilms, the formation of process consumes most of the charges along the polymers by electrostatic interaction, with only the surface charges remaining, resulting in a film with an overall low-charge density (**Figure 4a**). Thus, to increase the charge density of LbL nanofilms, preservation of the charges during film fabrication is essential. If this could be achieved, the nanofilms would be fully same type of charge, both inside and on the surface (**Figure 4b**). Due to the structure and charge distribution, the fully single-charged LbL nanofilms would be with higher charge density and show the pH responsiveness, makes them suitable for various applications like loading opposite-charged molecules or ions in biomedical and environmental fields.

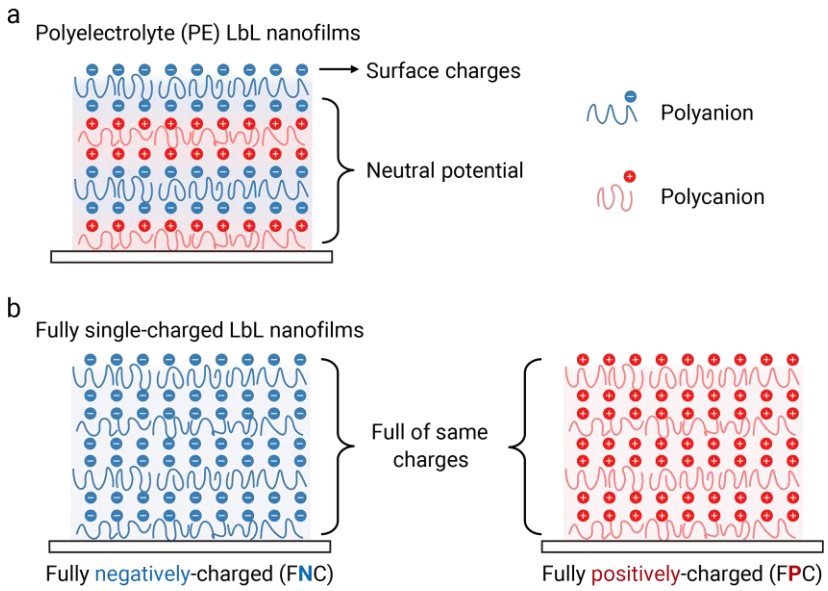

Figure 1-4 Structure and charge distribution of polyelectrolyte LbL nanofilms (a) and fully single-charged LbL nanofilms (b).

Because of electrostatic repulsion, PE with the same kind of charges cannot assemble directly so the key point is to introduce new covalent bonding to overcome the electrostatic repulsions. (**Figure 5a**) The click reaction can be conducted efficiently at room temperature and form the stable triazole. The new-formed covalent bonding improved the stability of fabricated nanofilms. Caruso had proved the successful application of Cu catalyst click reaction in preparing the LbL nanofilms.[51,52] So In this study, the click reaction would be introduced as the new driving force to overcome the electrostatic repulsions

To facilitate the LbL assembly, the electrostatic repulsion between same-charged PE can be reduced by changing the pH. As shown in **Figure 5b**, decrease the pH value for polyanions to partially protonate the anion groups and increase the pH for polycations to deprotonate the cation groups. After the assembly of nanofilms driven by stepwise crosslinking by the new covalent bond, the pH can be adjusted back to regain the charges along the polymer chains.

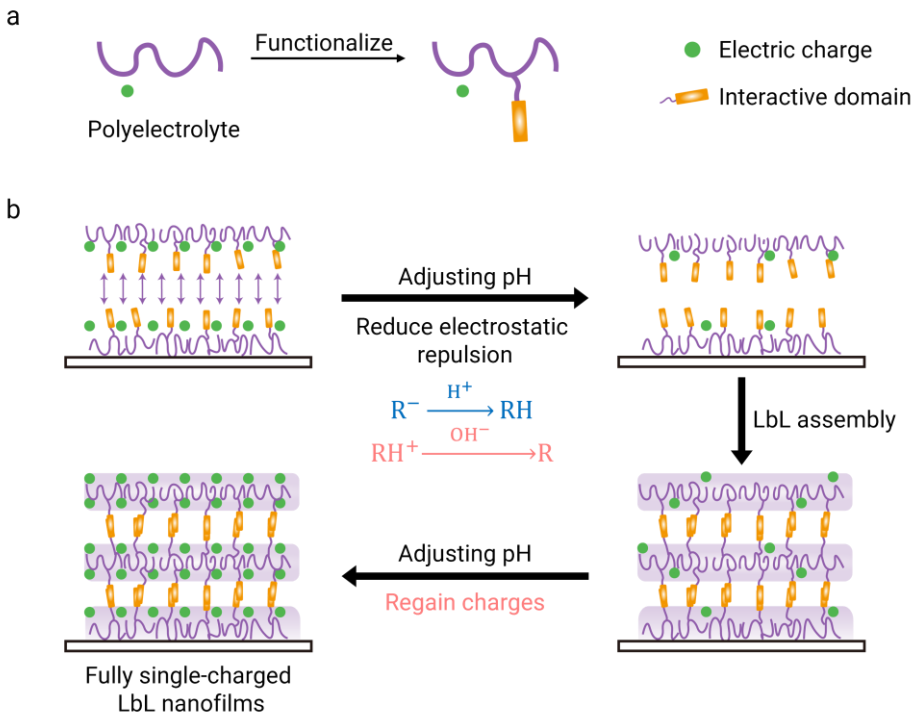

Figure 5 Schematic illustration of the fabrication of fully single charged LbL nanofilms by stepwise crosslinking. (a) Functionalization of polyelectrolyte. (b) Fully single charged LbL nanofilms fabrication.

Outline of this thesis

In this thesis, the author introduce the fabrication of a series of fully single-charged LbL assembled nanofilms between PE with same type of charge by stepwise crosslinking. This thesis includes the following three chapters

Chapter 1. Fabrication of fully negatively-charged LbL nanofilms

In this chapter, the fully negatively-charged (FNC) LbL nanofilms were fabricated using poly acrylic acid (PAA) as the polymer backbone. The nanofilms were assembly by stepwise crosslinking using copper-catalyzed azide-alkyne cycloaddition (CuAAC) click reaction as the new covalent bond. The yielded fully negative-charged (FNC) nanofilms possessing unique properties compared to conventional PE nanofilms, including high stability and reversible pH-induced remarkable swelling-shrinking properties in response to cyclic transitions between alkaline and acidic conditions.

Chapter 2. Fabrication of fully positively-charged LbL nanofilms

In this chapter, the fully positively-charged (FPC) LbL nanofilms were fabricated with poly-l-lysine as the main component and their characterizations were investigated. Similar to Chapter 1, the nanofilms were fabricated with all the individual layers covalently bonded, improving the pH stability. Because the resulting nanofilms had high charge density with positive charges both inside and on the surface, they show pH-dependent swelling properties and adsorption of negatively charged small molecules.

Chapter 3 In-situ LbL assembly of fully negatively-charged nanofilms on living cell surface

In this chapter, Cu-free fully negatively charged LbL nanofilms were successfully assembled on a living cell surface for the first time using only poly acrylic acid (PAA) by introducing Cu-free strain-promoted click chemistry to crosslink PAA layers. The film fabrication avoid the using of cytotoxicity of polycations. The resulting nanofilms retained their negative charges and showed higher adsorption of positively-charged molecules without affecting the cell viability.

References

[1] T. Çaykara, M. G. Sande, N. Azoia, L. R. Rodrigues, C. J. Silva, *Med. Microbiol. Immunol. (Berl.)* **2020**, *209*, 363.

[2] J. B. M. Rocha Neto, G. G. Lima, A. Fiamingo, L. G. L. Germiniani, T. B. Taketa, R. A. Bataglioli, G. A. T. da Silveira, J. V. L. da Silva, S. P. Campana-Filho, O. N. Oliveira, M. M. Beppu, *Int. J. Biol. Macromol.* **2021**, *172*, 154.

[3] W.-H. Chen, G.-F. Luo, W.-X. Qiu, Q. Lei, L.-H. Liu, S.-B. Wang, X.-Z. Zhang, *Biomaterials* **2017**, *117*, 54.

[4] J. Zheng, N. Rahman, L. Li, J. Zhang, H. Tan, Y. Xue, Y. Zhao, J. Zhai, N. Zhao, F. Xu, L. Zhang, R. Shi, Y. Lvov, J. Xue, *Mater. Sci. Eng. C* **2021**, *128*, 112295.

[5] R. K. Iler, *J. Colloid Interface Sci.* **1966**, *21*, 569.

[6] J. J. Kirkland, *Anal. Chem.* **1965**, *37*, 1458.

[7] S. Amorim, I. Pashkuleva, C. A. Reis, R. L. Reis, R. A. Pires, *J. Mater. Chem. B* **2020**, *8*, 3880.

[8] S. J. Gates, A. Shukla, *J. Polym. Sci. Part B Polym. Phys.* **2017**, *55*, 127.

[9] H. F. Alotaibi, Y. Al Thaher, S. Perni, P. Prokopovich, *Curr. Opin. Colloid Interface Sci.* **2018**, *36*, 130.

[10] N. E. Muzzio, M. A. Pasquale, D. Gregurec, E. Diamanti, M. Kosutic, O. Azzaroni, S. E. Moya, *Macromol. Biosci.* **2016**, *16*, 482.

[11] V. Panchagnula, J. Jeon, A. V. Dobrynin, *Phys. Rev. Lett.* **2004**, *93*, 037801.

[12] E. Guzmán, H. Ritacco, F. Ortega, R. G. Rubio, *Colloids Surf. Physicochem. Eng. Asp.* **2011**, *384*, 274.

[13] F. Croisier, G. Atanasova, Y. Poumay, C. Jérôme, *Adv. Healthc. Mater.* **2014**, *3*, 2032.

[14] J. Zeng, M. Matsusaki, *Polym. Chem.* **2019**, *10*, 2960.

[15] M. P. Sousa, I. Gonzalez de Torre, M. B. Oliveira, J. C. Rodríguez-Cabello, J. F. Mano, *Mater. Today Chem.* **2017**, *4*, 150.

[16] M. Yılmaz Aykut, A. del Barrio, C. M. Costa, S. Lanceros Méndez, J. C. Rodríguez-Cabello, J. L. Gómez Ribelles, M. Santos, G. Gallego Ferrer, *Eur. Polym. J.* **2021**, *146*, 110269.

[17] H. Yan, X. Chen, M. Feng, Z. Shi, D. Zhang, Q. Lin, *Mater. Lett.* **2017**, *209*, 492.

[18] T.-D. Zhang, X. Deng, Y.-F. Wang, X.-T. Wang, X. Zhang, L.-L. Chen, X. Cao, Y.-Z. Zhang, C.-Y. Zhang, X. Zheng, D.-C. Yin, *Appl. Surf. Sci.* **2020**, *530*, 147197.

[19] X. Wang, R. Wang, F. Wu, H. Yue, Z. Cui, X. Zhou, Y. Lu, *Eur. Polym. J.* **2021**, *158*,

110689.

[20] M. Kitsara, G. Tassis, A. Papagiannopoulos, A. Simon, O. Agbulut, S. Pispas, *Macromol. Biosci.* **2022**, *22*, 2100346.

[21] D. Yılmaz Aykut, Ö. Yolaçan, H. Deligöz, *Colloids Surf. Physicochem. Eng. Asp.* **2020**, *602*, 125113.

[22] Y. Qu, T. Wei, W. Zhan, C. Hu, L. Cao, Q. Yu, H. Chen, *J. Mater. Chem. B* **2017**, *5*, 444.

[23] F. Lv, L. Xu, Y. Zhang, Z. Meng, *ACS Appl. Mater. Interfaces* **2015**, *7*, 19104.

[24] T. He, D. Jańczewski, S. Guo, S. M. Man, S. Jiang, W. S. Tan, *Colloids Surf. B Biointerfaces* **2018**, *161*, 269.

[25] J. Woo, Y. Na, W. I. Choi, S. Kim, J. Kim, J. Hong, D. Sung, *Acta Biomater.* **2021**, *125*, 242.

[26] D. Hong, S. H. Yang, *Macromol. Res.* **2018**, *26*, 1185.

[27] M. B. Oliveira, J. Hatami, J. F. Mano, *Chem. – Asian J.* **2016**, *11*, 1753.

[28] Y. Choi, B. Phan, M. Tanaka, J. Hong, J. Choi, *ACS Appl. Bio Mater.* **2020**, *3*, 6556.

[29] T. Liu, Y. Wang, W. Zhong, B. Li, K. Mequanint, G. Luo, M. Xing, *Adv. Healthc. Mater.* **2019**, *8*, 1800939.

[30] C. R. Correia, S. Nadine, J. F. Mano, *Adv. Funct. Mater.* **2020**, *30*, 1908061.

[31] P. Gentile, I. Carmagnola, T. Nardo, V. Chiono, *Nanotechnology* **2015**, *26*, 422001.

[32] R. F. Fakhrullin, A. I. Zamaleeva, M. V. Morozov, D. I. Tazetdinova, F. K. Alimova, A. K. Hilmutdinov, R. I. Zhdanov, M. Kahraman, M. Culha, *Langmuir* **2009**, *25*, 4628.

[33] A. I. Zamaleeva, I. R. Sharipova, A. V. Porfireva, G. A. Evtugyn, R. F. Fakhrullin, *Langmuir* **2010**, *26*, 2671.

[34] R. F. Fakhrullin, Y. M. Lvov, *ACS Nano* **2012**, *6*, 4557.

[35] J.-Z. Wang, Z.-Q. Ding, F. Zhang, W.-B. Ye, *Mater. Sci. Eng. C* **2017**, *77*, 1247.

[36] B. J. Kim, H. Cho, J. H. Park, J. F. Mano, I. S. Choi, *Adv. Mater.* **2018**, *30*, 1706063.

[37] M. Matsusaki, K. Kadowaki, Y. Nakahara, M. Akashi, *Angew. Chem. Int. Ed.* **2007**, *46*, 4689.

[38] A. Nishiguchi, H. Yoshida, M. Matsusaki, M. Akashi, *Adv. Mater.* **2011**, *23*, 3506.

[39] C. Zhou, J. Zhou, X. Ma, D. Pranantyo, J. Li, L. Xu, V. X. Truong, *Mater. Sci. Eng. C* **2021**, *121*, 111828.

[40] A. vander Straeten, D. Lefèvre, S. Demoustier-Champagne, C. Dupont-Gillain, *Adv. Colloid Interface Sci.* **2020**, *280*, 102161.

[41] A. L. Becker, A. P. R. Johnston, F. Caruso, *Macromol. Biosci.* **2010**, *10*, 488.

[42] D. Kim, S. Cheong, Y. G. Ahn, S. W. Ryu, J.-K. Kim, J. Cho, *Nanoscale* **2016**, *8*, 7000.

[43] G. Decher, J.-D. Hong, *Makromol. Chem. Macromol. Symp.* **1991**, *46*, 321.

[44] G. Decher, *Science* **1997**, *277*, 1232.

[45] S. Guo, X. Zhu, X. J. Loh, *Mater. Sci. Eng. C* **2017**, *70*, 1163.

[46] T. Crouzier, K. Ren, C. Nicolas, C. Roy, C. Picart, *Small* **2009**, *5*, 598.

[47] M. Urairi, T. Tsuru, S. Nakao, S. Kimura, *J. Membr. Sci.* **1992**, *70*, 153.

[48] D. S. Salloum, J. B. Schlenoff, *Biomacromolecules* **2004**, *5*, 1089.

[49] L. Krasemann, B. Tieke, *Langmuir* **2000**, *16*, 287.

[50] V. Gribova, R. Auzely-Velty, C. Picart, *Chem. Mater.* **2012**, *24*, 854.

[51] G. K. Such, J. F. Quinn, A. Quinn, E. Tjipto, F. Caruso, *J. Am. Chem. Soc.* **2006**, *128*, 9318.

[52] G. K. Such, E. Tjipto, A. Postma, A. P. R. Johnston, F. Caruso, *Nano Lett.* **2007**, *7*, 1706.

Chapter 1 Fabrication of fully negatively-charged LbL nanofilms

1.1 Introduction

Layer-by-layer (LbL) assembly between polyelectrolytes is widely used due to the countless choice of materials and simplicity of electrostatic interactions formation. However, the formation of PE LbL nanofilms consumes most of the charges along the polymers by electrostatic interaction, with only the surface charges remaining, resulting in a film with an overall low-charge density. Thus, to increase the charge density of LbL nanofilms, preservation of the charges during film fabrication is essential. If this could be achieved, the nanofilms would be fully single charged, both inside and on the surface. Due to their high charge density, the fully single-charged LbL nanofilms would be suitable for various applications like loading positive molecules or ions in biomedical and environmental fields. In 2006, Caruso and his group reported LbL assembly between same-charged PE for the first time.[1–4] They studied how the fabrication parameters affect the film thickness, but there was no further investigation into the unique properties of fully single-charged LbL nanofilms.

Because of electrostatic repulsion, PE with the same kind of charges cannot assemble directly so the key point is to introduce new interactive domains to overcome this phenomenon. Copper-catalyzed azide-alkyne cycloaddition (CuAAC) is a substitute interaction and a very efficient reaction.[5] Previous reports have demonstrated that click reaction is a substitute driving force to fabricate polymeric LbL nanofilms, both on planar and microparticle substrates.[1,2,6–8] Owing to the fast reaction rates at room temperature and the formation of stable triazole, this click reaction should be well suited to the assembly of PE with the same charges. The combination of click reaction and LbL assembly provides a convenient method for preparing fully charged nanofilms with high charge density. To the best of our knowledge, the properties of the fully-charged nanofilms are as yet unexplored.

In this study, we report the fabrication of fully negative-charged (FNC) LbL nanofilms by CuAAC click reaction. The LbL nanofilms can be fabricated by alternately exposing the substrate to azide-grafted polyacrylic acid (PAA-EG_2-Azi) and alkyne-grafted polyacrylic acid (PAA-Alk). Although click reaction of PAA-Azi and PAA-Alk has already been reported, we newly synthesized PAA-EG_2-Azi to enhance water solubility in alkaline condition for homogeneous reaction. With the presence of Cu(I), the alkyne and azide groups will be catalyzed to form a stable triazole ring (Scheme 1a). The obtained nanofilms are denoted as

(PAA-EG_2-Azi/PAA-Alk)$_n$ (where n is the bilayer number). Due to the high content of carboxyl groups (-COOH) along PAA chains, the LbL nanofilms are fully negative-charged and can respond to pH changes (Scheme 1b). Additionally, compared to traditional PE LbL nanofilms between polycations and polyanions (Scheme 1c), our FNC nanofilms will not dissociate when pH changes. Briefly, our strategy takes advantage of the high efficiency of the CuAAC click reaction, suggesting a method to design fully-charged LbL nanofilms, with potential applications in the fields of functional nanomaterials such as sensors, actuators, diagnostics, and reactors.

1.2 Experiments

1.2.1 Materials

Poly (acrylic acid) (PAA, 25 kDa), boric acid (H_3BO_3, 99.5%), sodium hydroxide (NaOH, 93.0%), hydrochloric acid (HCl, 5 M), sulfuric acid (H_2SO_4, 95.0%), and disodium salt dihydrate (EDTA) were purchased from Wako Pure Chemical Industries, Ltd. 4-(4,6-Dimethoxy-1,3,5-triazin-2-yl)-4-methyl morpholinium chloride (DMTMM, 97.5%) was purchased from Watanabe. 2-[2-(2-azidoethoxy) ethoxy] ethanamine (Azide-EG_2-Amine, 95%) was purchased from BroadPharm. Propargylamide (Alkyne-Amine, >97%) was purchased from TCI. Copper (II) sulfate pentahydrate ($CuSO_4$•$5H_2O$), sodium L-ascorbate ($C_5H_7NaO_6$), and Poly(allylamine) solution (Mw ~15,000, 20 wt. % in H_2O) were purchased from Sigma-Aldrich. Hydrogen peroxide (H_2O_2, 35%) was purchased from Kishida Chemical Co., LTD.

1.2.2 Synthesis of PAA-EG_2-Azi

Azide-modified PAA was synthesized via DMTMM-mediated conjugation.[9–11] Briefly, PAA (60.0 mg, 0.83 mmol) was dissolved in 12 mL sodium borate buffer solution (pH 8.5, 0.5 M), to which DMTMM (460.8 mg, 1.66 mmol) was added and stirred for 10 min. Azide-EG_2-Amine in a 0.1 (14.5 mg, 0.083 mmol), 0.25 (36.3 mg, 0.21 mmol), and 0.5 (72.5 mg, 0.415 mmol) molar ratio (relative to the -COOH groups in PAA) was dissolved separately in sodium borate buffer solution (12 mL, pH 8.5, 0.5 M). This solution was then added dropwise to the PAA solution. The reaction was conducted at room temperature for 24 h and then the solution was dialyzed against Milli-Q water for 3 days (MWCO: 7000 Da, Thermo Fisher Scientific). After dialysis, PAA-EG_2-Azi was obtained by lyophilization.

1.2.3 Synthesis of PAA-Alk

PAA functionalized with alkyne was also prepared via DMTMM conjugation in Milli-Q water. Briefly, PAA (60.0 mg, 0.83 mmol) was dissolved in 12 mL Milli-Q water. After completely dissolving, DMTMM (460.8 mg, 1.66 mmol) was added to the PAA solutions and stirred for 10 min. Alkyne-amine solutions in a 0.20 (9.17 mg, 0.166 mmol), 0.35 (16.1 mg, 0.291 mmol), and 0.5 (22.9 mg, 0.416 mmol) molar ratio (relative to the -COOH groups in PAA) was dissolved in Milli-Q water (12 mL) and transferred dropwise. The pH was adjusted to 5.5 with additions of 0.1 M HCl. The reaction was conducted at room temperature for 24 h. The product was purified by dialysis (MWCO: 7000 Da, Thermo Fisher Scientific) against Milli-Q water for 3 days and lyophilized.

1.2.4 Monitoring the layer-by-layer (LbL) nanofilm fabrication

The FNC nanofilm fabrication was monitored by 27 MHz quartz crystal microbalance (QCM) (AFFINIX Q8, ULVAC). QCM sensors coated with gold (QCM01S, ULVAC) were treated with Piranha solution (H_2SO_4:35% H_2O_2 = 3:1) for 10 min and repeated 3 times. After rinsing the sensor with Milli-Q water 3 times, 100 μL of Cu(I) solution (pH 3.5, 0.36 mg/mL $CuSO_4$, 0.88 mg/mL SA) at 25 °C were added into the cells until the frequency reached a steady state. 5 μL PAA-EG_2-Azi solutions were added to the cells, and frequency changes were monitored. After 15 min of deposition, sensors were rinsed with Milli-Q water (pH 3.5) 3 times and equilibrated in 100 μL of Cu(I) solution. 5 μL PAA-Alk solutions were injected into the cells for the second layer deposition. By alternately changing the polymer solutions in cells, nanofilms via layer-by-layer assembly were fabricated. For film fabrication without Cu(I), the $CuSO_4$ solution was replaced with Milli-Q water (pH 3.5). For nanofilm fabricated at pH 9, the pH of all the solutions used will be adjusted to 9. For nanofilms fabricated without Cu(I), the $CuSO_4$ will not use.

For the fabrication of (PAA/PAA-Alk) and (PAA-EG_2-Azi/PAA) LbL nanofilms, one of the functionalized polymers was replaced with PAA (0.16 mg/mL, pH 3.5) and the same protocol was followed. To fabricate polyelectrolyte (PE) LbL nanofilms composed of PAH and PAA, QCM sensors were treated with the same method as previously described. 100 μL of Milli-Q water was added into the cells until a stable frequency was attained. 5 μL PAH solution was added into the cells and deposited for 15 min, then rinsed with Milli-Q water 3 times. When a stable frequency was again attained, 5 μL PAA solution was injected into the cells for the second layer deposition. By alternating PAA and PAH solutions in cells, PE

nanofilms were deposited on the sensor, and the fabrication process was monitored by QCM.

The deposited mass (Δm) was calculated with the Sauerbrey equation.[12] A frequency change of 1 Hz corresponded to a mass change of 0.62 ng cm^{-2} in the QCM system used here (Equation 1-1).

$$-\Delta m(\mathrm{ng/cm^2}) = 0.62\Delta F(\mathrm{Hz}) \qquad (1-1)$$

Based on the depostied mass (Δm) and an assumed polymer density of 1.2 g/cm^3,[13] the thickness of the resultant nanofilm was calculated according to the equation 1-2.

$$Thickness(nm) = \frac{\Delta m(ng/cm^2)}{1.2 \times 10^2} \qquad (1-2)$$

1.2.5 Characterization of FNC LbL nanofilms

The pH-responsive measurement and stability evaluation of LbL nanofilms were accessed in situ by QCM. After film fabrication, they were incubated in 100 μL solutions with different pH that adjusted only using HCl or NaOH.

The adsorption properties of FNC nanofilms were evaluated using methylene blue (MB) and measured by QCM. After nanofilms LbL assembly on the QCM sensors, they were kept in 100 μL Milli-Q (pH 3.5), then 5 μL MB solutions at pH 3.5 would be added to make the nanofilms exposed to diluted MB solutions with a concentration of 10 μg/mL.

1.2.6 Surface zeta potential measurement

LbL nanofilms for surface zeta potential measurement were deposited on glass slides which were cut into 4 mm × 7 mm shapes. The nanofilms were fabricated via standard dip assembly protocols. After cleaning the substrates with Piranha solution 3 times. substrates were alternately immersed into PAA-EG_2-Azi (pH 3.5, 0.16 mg/mL) solution and PAA-Alk (pH 3.5, 0.16 mg/mL) solution containing Cu(I). Between each step, substrates were rinsed with Milli-Q water (pH 3.5). Surface zeta potential measurement was performed using a Zetasizer Nano ZS (Malvern, U.S.A) with a dip cell (ZEN1020), which is composed of a 4 mm sample stage that is positioned between two small electrodes and placed in a cuvette filled with the dispersant and tracer particles (PS NPs 0.25 μm, 0.0005% w/v). The vertical position of the sample stage was moved with respect to the detection optics by the adjuster at the cell top. The tracer mobility measurement was collected at five increasing displacements

from the surface: 135, 250, 375, 500, and 625 μm. The electrophoretic mobility of the tracer particle was measured at a position far from the sample stage. After the measurement, the surface zeta potential was provided by the Zetasizer software.

1.2.7 AFM and SEM observation

Nanofilms for AFM and SEM observation were fabricated on silicon wafers. Before the film fabrication, silicon wafers were treated with plasma for 10 min and then immersed in PEI solution (1 mg/mL) for 15 min to make the surface positive-charged, then the nanofilms were fabricated following the same protocol as on the glass substrate. The top surface morphologies and roughness of LbL nanofilms with different post-treatments were investigated at different pH conditions such as pH 2, pH 6-8 (Milli-Q water), and pH 12 solutions by AFM (Dry: JEOL, JSPM-5400; Wet: SHIMADZU, SPM-Nanoa). The cross-section of the nanofilms were observed by SEM (JEOL, JSM-6701F). All nanofilms used for AFM and SEM measurement were assembled into 10 bilayers for better observation.

1.2.8 Characterization methods

Chemical structure analysis of polymers was performed by FT-IR (HORIBA, FT-720, Japan) over a range of 4000-650 cm^{-1} and ^{1}H-NMR (JEOL, JNM-GSX 400, Japan)

1.3 Results and discussion

1.3.1 Synthesis of PAA-EG_2-Azi and PAA-Alk

The reactions used to synthesize PAA-EG_2-Azi and PAA-Alk are illustrated in Figure S1. Briefly, both PAA-EG_2-Azi and PAA-Alk were synthesized by grafting azide and alkyne onto the carboxyl (-COOH) groups of PAA. ^{1}H-NMR confirmed the structure of the obtained polymer (**Figure 1-1a**). For PAA-EG_2-Azi, the peaks observed in the range 3.2-4.0 ppm represent the existence of an azide moiety, and broad peaks in the range 2.5-1.5 ppm correspond to the PAA polymer chain. The graft degree of alkyne was calculated by integrating the area under the PAA peaks and azide moiety, as shown in Figure S2. In a similar manner, the peaks observed at 3.94 and 2.60 ppm correspond to the three protons of an alkyne moiety. Also, the graft degree was calculated by the integral area of the alkyne moiety and polymer chain signals (**Figure 1-1b and c**). To distinguish PAA with different graft degrees, functionalized polymers are named by their graft degree as a subscript. For azide-modified PAA, they were named as PAA-EG_2-Azi_{11}, PAA-EG_2-Azi_{21}, and PAA-EG_2-Azi_{41} (**Figure 1-1b**). For alkyne-modified PAA, they were named as PAA-Alk_5, PAA-Alk_{20}, and

PAA-Alk$_{31}$ (**Figure 1-1c**).

a

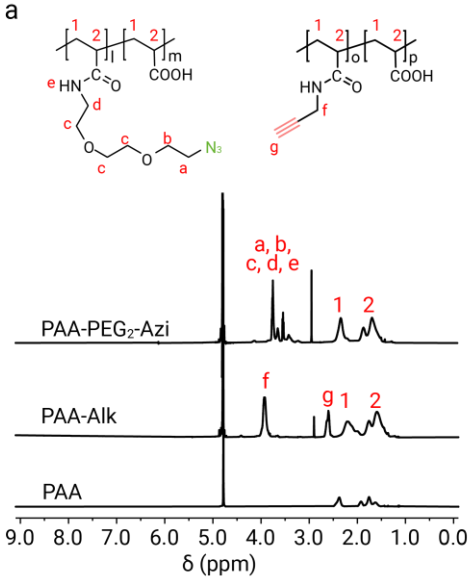

b

Polymer	-COOH (eq.)	-Azi (eq.)	Graft degree# (%)	Yield (%)
PAA-EG$_2$-Azi$_{41}$	1.0	0.50	41	85
PAA-EG$_2$-Azi$_{21}$	1.0	0.25	21	91
PAA-EG2-Azi$_{11}$	1.0	0.10	11	85

c

Polymer	-COOH (eq.)	-Alk (eq.)	Graft degree# (%)	Yield (%)
PAA-Alk$_{31}$	1.0	0.50	31	78
PAA-Alk$_{20}$	1.0	0.35	20	46
PAA-Alk$_5$	1.0	0.20	5	83

Figure 1-1 (a) ^{1}H-NMR (400 MHz, D$_2$O, 25 °C) spectra of PAA, PAA-EG$_2$-Azi, and PAA-Alk. (b-c) Molar ratio and graft ratio of PAA-EG$_2$-Azi (b) and PAA-Alk (c). #Graft degree was calculated by ^{1}H-NMR

1.3.2 Fabrication of fully negatively-charged (FNC) LbL nanofilms

As shown in **Figure 1-2a**, the fabrication of FNC layer-by-layer nanofilms was driven by copper-catalyzed click reaction (CuAAC) between the azide groups in PAA-EG$_2$-Azi and the alkyne groups in PAA-Alk. The irreversible formation of triazole leads to the absorption of one polymer by another one. To facilitate the LbL assembly, the pH of all solutions was adjusted to 3.5 to protonate carboxyl groups, thus reducing the electrostatic repulsion between polymer chains. The LbL assembly started with PAA-EG$_2$-Azi on substrates treated with Piranha solution, followed by the addition of PAA-Alk with the existence of Cu(I). During this process, the reaction between Azi and Alk formed triazole, together with the formation of hydrogen bond between protonated carboxyl groups at pH 3.5, result in a simultaneous attachment of the PAA-Alk layer to the underlying PAA-EG$_2$-Azi layer. Thus, one bilayer was successfully prepared. This process was then repeated by alternately immersing substrates into PAA-EG$_2$-Azi and PAA-Alk solutions. To facilitate the LbL assembly, the pH of all solutions was adjusted to 3.5 to protonate carboxyl groups, thus reducing the

electrostatic repulsion between polymer chains.

The stepwise LbL assembly of the nanofilms was monitored by quartz crystal microbalance (QCM) (**Figure 1-2b**). As expected, when polymers were added, the frequency decreased due to the adsorption of PAA-EG$_2$-Azi or PAA-Alk. After 15 min, the adsorption of polymers on the sensors reached saturation and the frequency remained constant. The sensors were then rinsed with pH 3.5 Milli-Q water, at which point the frequency increased, indicating the wash-away of some weakly attached polymers. The film thickness can be tailored by adjusting the graft degree of functional groups. **Figure 1-2c** shows the negative frequency shift (-ΔF) and film thickness at each assembly step. Thicker films were observed with increasing graft degree and the film thickness increased from approximately 18 nm to 393 nm. Thicker films can be attributed to an increasing driving force due to more click moieties along polymer chains with higher graft degrees. The thickness of the FNC nanofilms can be finely tuned in nanometer scale by adjusting both graft ratio and assembly steps.

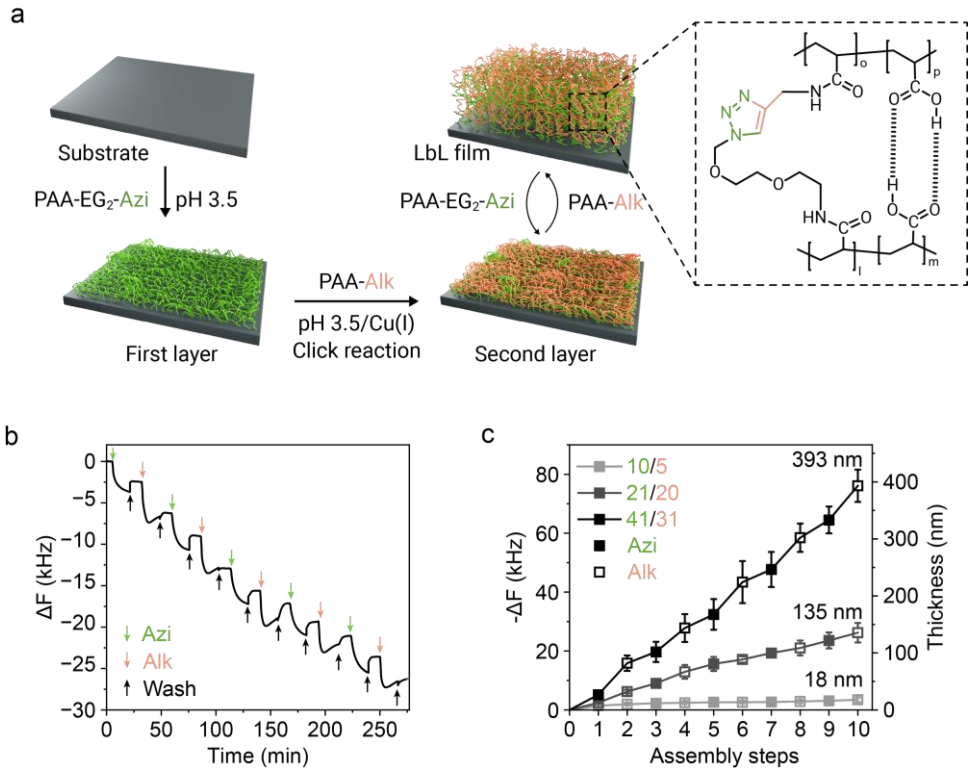

Figure 1-2 (a) Schematic illustration of FNC LbL nanofilms fabrication via click reaction. (b) Frequency shifts (ΔF) plotted against time for (PAA-EG$_2$-Azi$_{21}$/PAA-Alk$_{20}$)$_5$ LbL nanofilms assembly with a polymer concentration of 0.16 mg/mL. Vertical arrows indicate the

beginnings of polymer exposure and washing with Milli-Q (pH 3.5) at the end of polymer exposures. (b) Frequency shift and thickness increase of $(PAA\text{-}EG_2\text{-}Azi/PAA\text{-}Alk)_5$ LbL nanofilms assembled by polymers with different graft ratios ($n \geq 3$). The concentration of polymer solutions was 0.16 mg/mL.

1.3.3 Confirmation of stepwise crosslinking

To confirm the stepwise crosslinking during the LbL nanofilm fabrication, the click reaction between azide and alkyne was proved through the observation of changes in the ^{1}H-NMR spectra of Alkyne-Amine and Azide-EG_2-Amine monomers (**Figure 1-3a**). As shown in **Figure 1-3b**, the conversion of both monomers in the click reaction leads to the decrease in intensity of monomer signals and the appearance of new peaks. Specifically, peaks at 4.64 (peak 6') and 4.00 (peak a') were attributed to the adjoining protons of the newly formed triazole ring.[14]

Furthermore, to demonstrate stepwise crosslinking during nanofilm fabrciation, PAA-EG_2-Azi/PAA-Alk LbL nanofilms without Cu(I) were also fabricated for comparison (Figure S6). Even though there was no catalyst for click reaction, nanofilm deposition was still observed by QCM. We assumed that hydrogen bonds between polymers may serve as the driving force for LbL assembly. Urea (4 M) was then added, which can participate in the formation of strong hydrogen bonds and is normally used as the breaker of relatively weak hydrogen bonds between polymers.[15–17] As shown in **Figure 1-3**, for LbL nanofilms assembled with Cu(I), the addition of urea didn't make the nanofilms dissociate, this is because even urea break the hydrogen bonding between polymers, the covalent bonds formed during nanofilms fabrication maintain the structure of nanofilms (**Figure 1-3c-i**). The remaining weight even increased after incubating in urea solutions, this is because the pH increases of 4M urea solution (pH 7.95) from the fabrication condition (pH 3.5). However, for nanofilms fabricated without Cu(I), there is no stepwise crosslinking, so an immediate degradation nanofilms without Cu(I) observed (**Figure 1-3c**) after the hydrogen bond being broken (**Figure 1-3c-ii**).

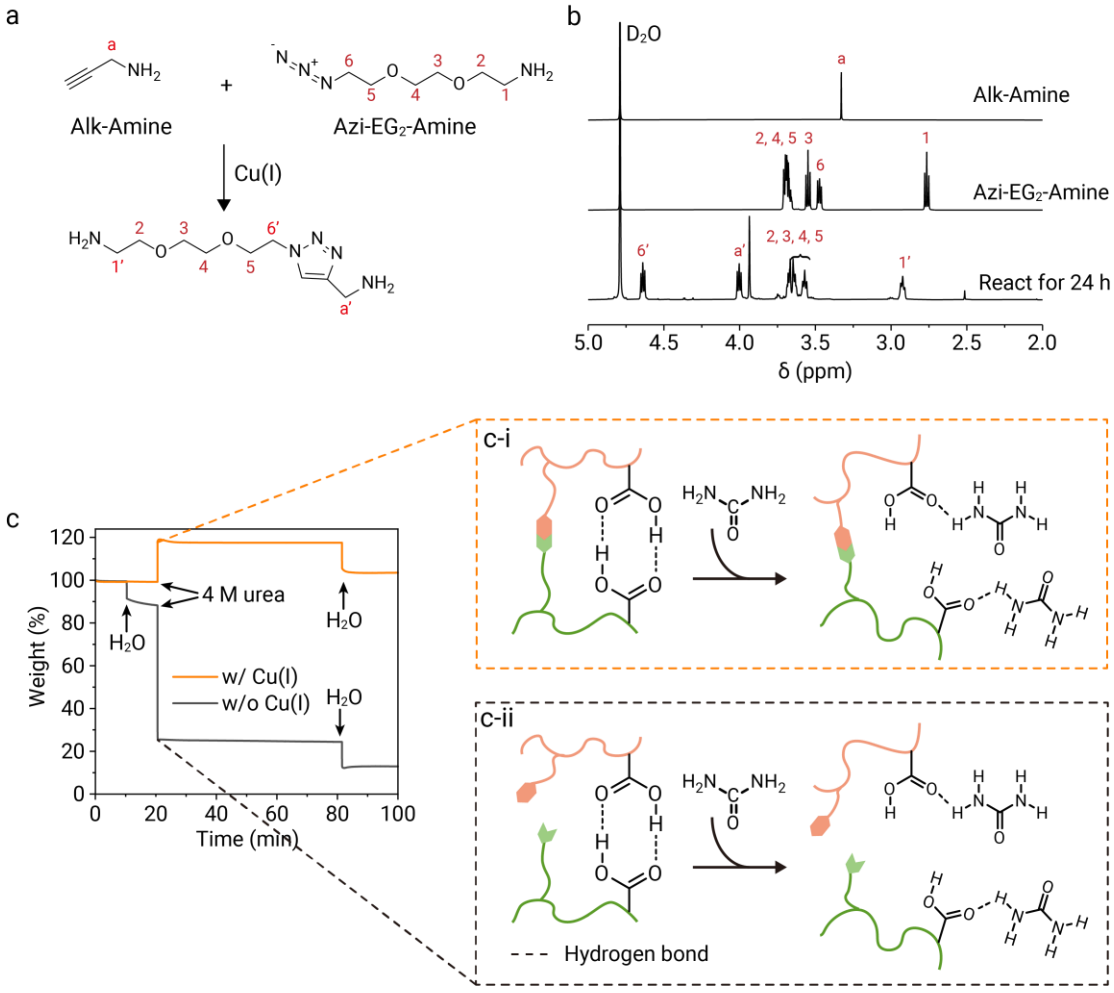

Figure 1-3 (a) The click reaction between Alk-amine and Azi-EG$_2$-Amine with Cu(I) as catalyst. (b) ^{1}H-NMR spectra of Alk-Amine, Azi-EG$_2$-Amine, and the product after reacting for 24 hours (400 Hz, 25 °C, D$_2$O). (c) Left: stability of (PAA-EG$_2$-Azi$_{21}$/PAA-Alk$_{20}$)$_5$ LbL nanofilms fabricated w/ or w/o Cu(I) in urea solution (4 M, pH 7.95). Arrows indicate the addition of H$_2$O or urea. Right: schematic illustrations demonstrate how urea breaks the hydrogen bonds in LbL nanofilms fabrication w/ (c-i) and w/o (c-ii) Cu(I).

1.3.4 pH effect on FNC LbL nanofilm fabrication

As aforementioned mechanism, pH affects the electrostatic repulsions between polymers and then influences the LbL assembly. Here the pH effect on FNC nanofilm fabrication was investigated under three different conditions: (i) w/ Cu(I), (ii) w/ Cu(I) pH 9, and (iii) w/o Cu(I) pH 9, the results were shown in **Figure 1-4**. At condition (i), when the nanofilms were fabricated with Cu(I) at pH 3.5, there are both covalent bonding and hydrogen bonding between the polymers (**Figure 1-4a-i**), the combination of these interactions resulted in the

nanofilms with a thickness of 393 nm. At the condition (ii), when the pH increased to 9, the carboxyl groups being deprotonated, generating electrostatic repulsions between the polymers (**Figure 1-4a-ii**). The decrease in total interactions between the polymers resulted in the nanofilms thickness reducing to 141 nm. However, at condition (iii), when there is no Cu(I) as catalyst and at pH 9, no interactions occurred between the polymers, so the nanofilms could not be assembled under this condition (**Figure 1-4a-iii**). These results proved that the lower pH helps the nanofilms assembly by reducing the electrostatic repulsion between the polymers and confirm the critical role of stepwise crosslinking again in the nanofilms fabrications.

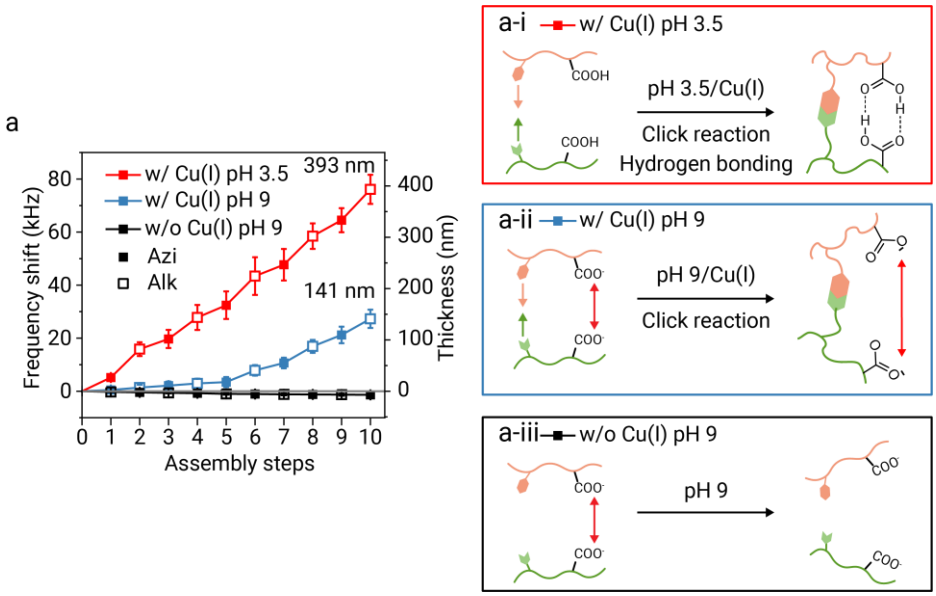

Figure 1-4 (a) $(PAA\text{-}EG_2\text{-}Azi_{41}/PAA\text{-}Alk_{30})_5$ nanofilms fabricated at three different conditions and the corresponding illustration show the LbL assembly behaviors. (a-i) w/ Cu(I) pH 3.5, (a-ii) w/ Cu(I) pH 9, and (a-iii) w/o Cu(I) pH 9.

1.3.5 pH stability of FNC LbL nanofilms

The stability of the traditional PE LbL nanofilms is generally limited because electrostatic interactions can be easily influenced by external stimuli, especially the pH changes.[18,19] Here the pH stability of the FNC LbL nanofilms were investigated. both FNC nanofilms and PE nanofilms were fabricated using polymers with the same concentration (0.16 mg/mL) (**Figure 1-5a**). After the film fabrication, LbL nanofilms were incubated in pH 2 and pH 12 solutions, respectively, and then the remaining weight (%) of each nanofilm was recorded. As shown in **Figure 1-5b**, PE LbL nanofilms incubated in pH 2 and pH 12 solutions

both dissociated rapidly in the first hour, the remaining weight (%) decreased to 40%. After the first hour, PE nanofilms incubated in pH 12 solutions stayed stable until the end of the measurement. But in the pH 2 solution, PE nanofilms slowly dissociated and the remaining weight (%) of PE nanofilms decreased to 29% after incubation for 8.8 h. In contrast, FNC nanofilms showed long-term stability during the entire measurement, both in acidic and alkaline solutions. The pH stability of FNC nanofilms was attributed to the triazole linkages between adjacent layers, which can resist the pH changes.[20] PE nanofilms are simply cohered by electrostatic interactions, which can be easily destroyed when the charges are eliminated in harsh pH conditions.[21] Without the main electrostatic interactions between polycations and polyanions, the PE nanofilms can be easily dissociated.

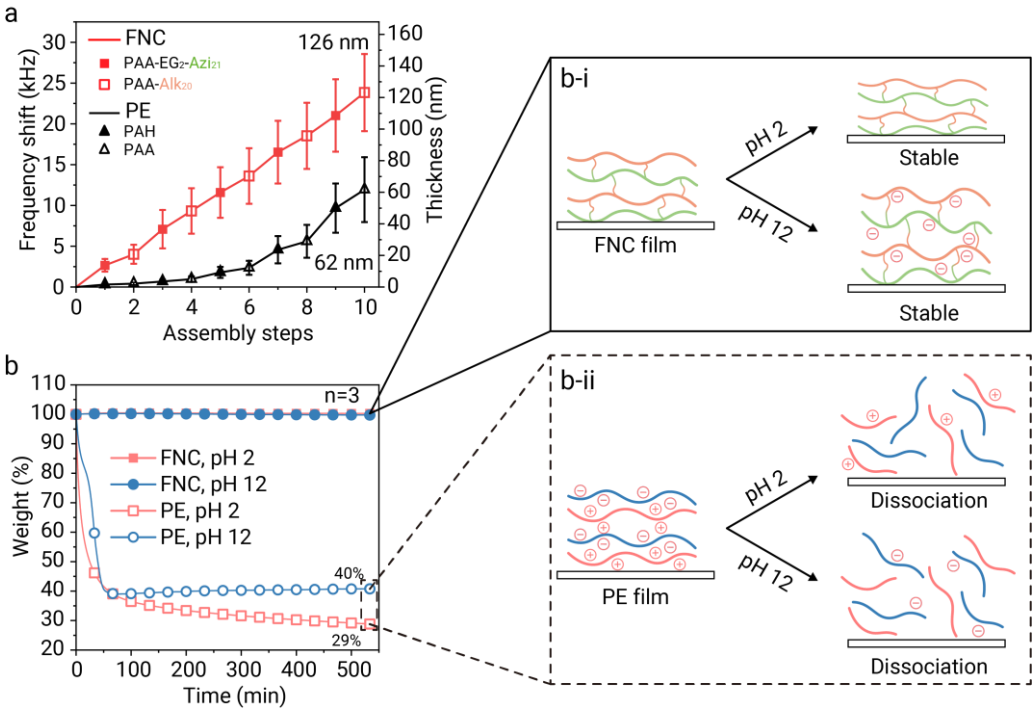

Figure 1-5 (a) Frequency shift and thickness increasing of $(PAA\text{-}EG_2\text{-}Azi_{21}/PAA\text{-}Alk_{20})_5$ FNC LbL nanofilms and $(PAH/PAA)_5$ PE LbL nanofilms for the pH stability measurement. All the polymers used are with the same concentration of 0.16 mg/mL. FNC nanofilms were fabricated at pH 3.5, PE nanofilms were fabricated in Milli-Q water. (b) Stability of FNC nanofilms and PE nanofilms when incubating in pH 2 and pH 12 solutions and illustration of the FNC (b-i) and PE (b-ii) nanofilms response to different pH during the incubation.

1.3.6 Charge distribution of FNC nanofilms

To demonstrate that the FNC nanofilms are able to preserve negative charges during the

film fabrication, surface zeta potentials at each assembly step were measured. As shown in **Figure 1-6**, for PE LbL nanofilms, when PAH was on the surface, the potential was positive, while the deposition of PAA decreased the surface potential. PAH/PAA nanofilms flipped the surface charge after depositing a new layer, showing a zig-zag curve, which is indicative of film fabrication through electrostatic interactions,[22,23] and also confirms the consumption of charges during the film fabrication. However, a different phenomenon was observed for FNC nanofilms. After alternately depositing different functionalized PAA to form FNC nanofilms, the surface charge remained negative all the time, indicating that FNC nanofilms could preserve the negative charges after deposition of a new layer, making the inside of the films also negatively charged after the film fabrication.

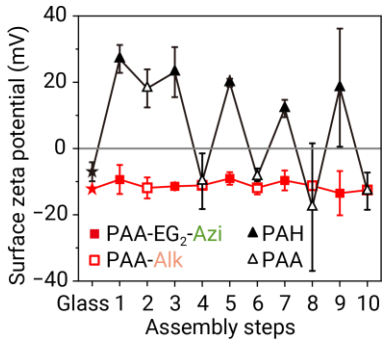

Figure 1-6 Surface zeta potential of FNC nanofilms and PE nanofilms (n = 3). LbL nanofilms were assembled on glass sheets. FNC nanofilms were fabricated using PAA-EG_2-Azi_{41} and PAA-Alk_{31} with a concentration of 0.16 mg/mL. PE nanofilms were fabricated using PAA and PAH solutions with a concentration of 1 mg/mL. Tris buffer (0.05 M, pH 7.4) was used as a dispersant, Nile red-Polystyrene (0.25 μm, 0.0005% w/v) was used as tracer particles.

1.3.7 pH responsiveness properties of FNC LbL nanofilms

Based on the structure and composition of the film, the FNC nanofilms are full of carboxyl groups, which are responsive to pH changes.[24] So we can infer our FNC nanofilms possess pH-responsive properties. The pH stabilities reported in the last section also allow us to take the measurement. The influence of pH on LbL nanofilms was investigated by QCM. After the fabrication, LbL nanofilms were incubated in different pH solutions, and the corresponding frequency was recorded from which thickness was calculated. The results are shown in **Figure 1-7a**, the film thickness was positively correlated with the pH values and showed different sensitivity to pH changes. At low pH, the thickness changed slowly as pH increased until 5, then the film thickness responded much more sensitively to the pH change

between pH 5-8. Then the thickness response to pH change becomes less sensitive again. The variation in film thickness can be associated with the protonation and deprotonation of carboxyl groups in the FNC nanofilms. An increase in pH causes ionization of carboxyl groups and then generates electrostatic repulsion and makes the nanofilms swell. At low pH, the carboxyl groups in the nanofilms become protonated and eliminate the electrostatic repulsion, so the swollen films collapse to the shrunken state. It is noteworthy that the thickness change is repeatable. FNC nanofilms were alternately incubated in pH 2 and pH 12 solutions. Every time the pH was changed, the frequency changed alongside the pH changes (Figure S12a). The frequency data was converted to film thickness based on the Sauerbrey equation.[25] This is because the films were covalently bonded and the triazole linkages prevent the films from dissociating in the harsh pH environment, endowing them with the reversible thickness change property (**Figure 1-7b**). Similar pH-induced thickness change behaviors were observed in FNC LbL nanofilms fabricated by polymers with different graft degrees. What can be clearly seen is that the thickness of all FNC nanofilms in the alkaline environment is greater than in the acidic environment due to the different states of carboxyl groups. We calculated the film swelling ratio from pH 2 to pH 12 according to the following equation:

$$\text{Swelling ratio (\%)} = \frac{Th_{12}}{Th_2} \times 100\%$$

Where Th_{12} and Th_2 represent film thickness at pH 2 and 12 solutions, respectively.

The results are shown in **Figure 1-7c**, the swelling ratio of FNC nanofilms were 238%, 201%, and 129% from the lowest to the highest graft degree. More marked thickness changes were observed with decreasing graft degree. Since the lower graft degree retains more carboxyl groups, the density of ionic carboxyl groups is higher, resulting in a more sensitive response to pH change. At the same time, the crosslinking density of the films fabricated by lower graft degree is also lower, making the nanofilm more flexible to swell.

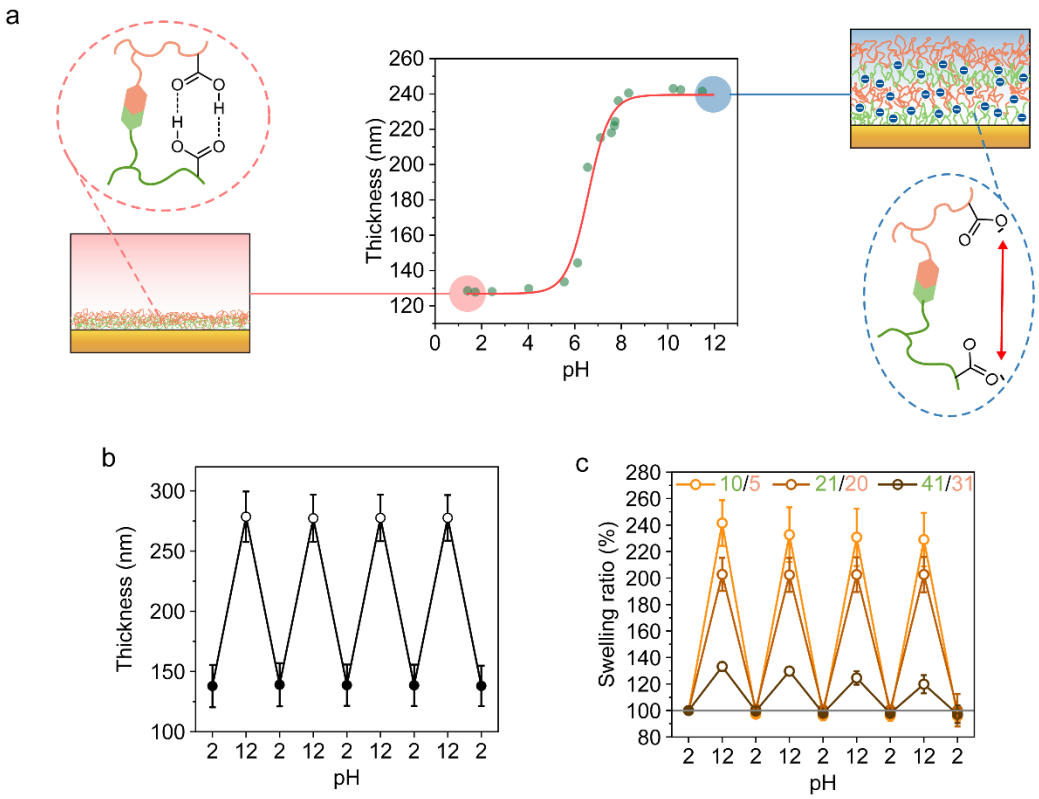

Figure 1-7 Thickness change of FNC LbL nanofilms. (a) Relationship between film thickness and pH values at the range of 2 to 12 and corresponding schematics depicting the swelling and shrinking of FNC LbL nanofilms. (b) Reversible thickness change of $(PAA\text{-}EG_2\text{-}Azi_{21}/PAA\text{-}Alk_{20})_5$ FNC nanofilms at pH 2 and pH 12 ($n \geq 3$). (c) Swelling ratio of FNC nanofilms fabricated by polymers with different graft degrees when the pH changed from 2 to 12 ($n \geq 3$). The concentration of polymer solutions was 0.16 mg/mL.

Surface morphologies of nanofilms play an important role in their applications. Tunable surface morphologies can be used to adjust the hydrophilicities, mechanical properties, and adsorption properties of the nanofilms. Hence, we investigated how the pH affects the surface properties of FNC LbL nanofilms. We used the $(PAA\text{-}EG_2\text{-}Azi_{21}/PAA\text{-}Alk_{20})$ FNC nanofilms for the investigation because of their relatively obvious magnitude of thickness change and high swelling ratio. After FNC nanofilm fabrication, films were washed with EDTA solutions to remove remained Cu ions followed by washing with Milli-Q water at pH 2 and pH 12, respectively. The EDTA washing step was also monitored by QCM as well as the pH responsive properties followed by EDTA washing. EDTA washing didn't affect the thickness of nanofilms, and the FNC nanofilms show pH-induced thickness change with a swelling ratio of 181% **(Figure 1-8)**, similar to the FNC nanofilms without EDTA washing.

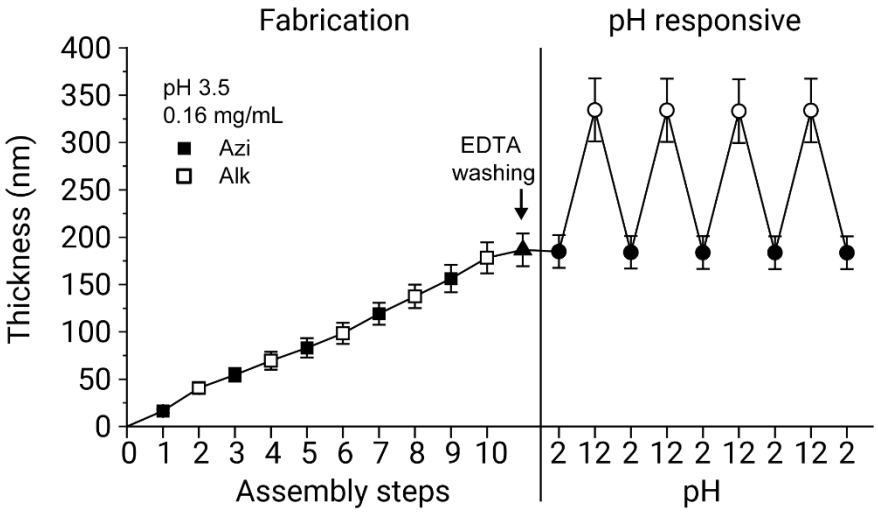

Figure 1-8 Thickness increasing of FNC LbL nanofilms followed by EDTA (0.1 M, 100 μL) washing and film thickness at pH 2 and pH 12 by QCM.

The surface morphologies of FNC nanofilms were measured by AFM (**Figure 1-9**). In agreement with the decreasing ionic degree of carboxyl groups in more acidic conditions, LbL nanofilms treated with lower pH showed increased roughness due to increased coiling of the polymer chains. The surface roughness was expressed by the value of Ra (arithmetic mean deviation). This is seen by AFM image of nanofilms in pH 2 solution, which exhibits bumps on the film surface (**Figure 1-9a**) and much larger Ra (5.0 nm) compared with nanofilms in Milli-Q water (0.3 nm) and pH 12 (0.2 nm) solutions. This change in surface roughness is attributed to the polymer backbone configurations. At low pH, polymer chains form more granular conformation as the decreased degree of ionization decreases interpolymer repulsion,[26,27] forming the collapsed polymer conformation and resulting in the agglomerates surface morphology. While at high pH, polymer chains tend to be more swollen, and the agglomerates disappear, resulting in a more homogeneous surface.

Nanofilms treated with different pH solutions were dried in air and measured by AFM again (**Figure 1-9c**). The films showed a similar trend as in liquid. Obvious bumps can be observed from film dried from pH 2 solutions, while films dried from Milli-Q water and pH 12 solutions are more homogeneous. The increase in roughness of the dried films compared to films in the wet state may be attributed to the collapse of polymer chains in the air, which leads the films to buckle. The Ra of the films dried from pH 2, Milli-Q, and pH 12 increased to 53.3, 32.7, and 28.6 nm, respectively. Similar to the films in wet conditions, after film

drying, the film treated with pH 2 solution showed a rougher surface than the films treated with Milli-Q water and pH 12 solutions. Meanwhile, the difference in roughness also affects the photonic properties of the nanofilm. Since films treated with Milli-Q and alkaline solutions are more homogeneous, structure color can be observed from nanofilms dried in Milli-Q water and pH 12 solutions but not from nanofilms dried from the pH 2 solution (**Figure 1-9d**). Structure color is caused by the light interference effect. Because of the difference in the refractive index, the light is reflected by the upper and lower interfaces of the nanofilm. Then these two beams of light will interfere with each other, resulting in a brighter and more saturated structural color.[28] So for light interference, light should propagate through a homogeneous matrix with an effective refractive index (RI).[29–31] The structure color observed from neutral and alkaline environments demonstrates the homogeneity of the nanofilms. Furthermore, the observation of distinct structure color indicates differences in nanofilm thickness between those treated under neutral and alkaline conditions. Nanofilms treated with Milli-Q exhibit blue color, while those treated with pH 12 solutions show red color. According to Bragg's diffraction equation, an increase in film thickness leads to a red shift of structure color[32]. This is confirmed by cross-sectional SEM images in **Figure 1-9e**, showing that nanofilms treated with pH 12 solutions have a thickness of 255 nm, thicker than the nanofilms treated with Milli-Q with a thickness of 133 nm. Although SEM images were taken under vacuum conditions, which might result in thinner films compared to the regular atmosphere environment, the obtained SEM images represented the similar trend to that showed in structural color.

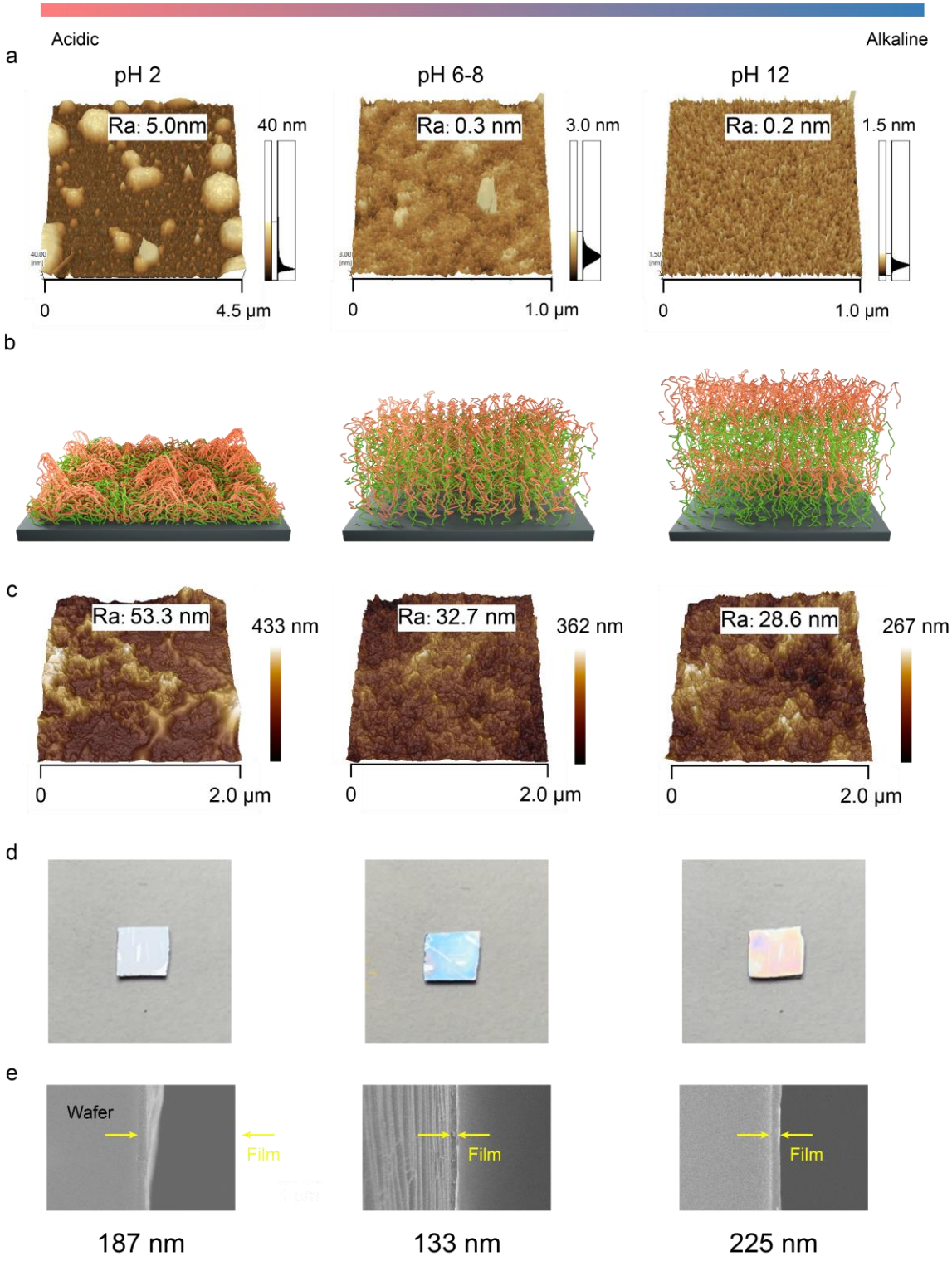

Figure 1-9 Surface morphology properties. (a) AFM images of $(PAA\text{-}EG_2\text{-}Azi/PAA\text{-}Alk)_{10}$ LbL nanofilms in pH 2, pH 6-8 (Milli-Q), and pH 12 solutions. (b) Schematic illustration of nanofilm structure in different pH conditions. (c) AFM images of $(PAA\text{-}EG_2\text{-}Azi/PAA\text{-}Alk)_5$ LbL nanofilms air-dried form pH 2, pH 6-8 (Milli-Q), and pH 12. (d) Structure color observed from air-dried $(PAA\text{-}EG_2\text{-}Azi/PAA\text{-}Alk)_{10}$ LbL nanofilms from pH 2, pH 6-8 (Milli-Q), and pH 12 solutions. Nanofilms were assembled onto PEI-coated silicon wafers by adsorbing

PAA-EG_2-Azi_{21} (0.16 mg/mL) and PAA-Alk_{20} (0.16 mg/mL) for 15 min per layer. Before being treated with different pH solutions, films were washed with EDTA (0.1 M) solution for the removal of Cu ions. (e) SEM cross section images of (PAA-EG_2-Azi/PAA-Alk)$_{10}$ LbL nanofilms deposited on silicon wafer. The nanofilms were treated with pH 2, Milli-Q, and pH 12 solutions then dry in the air at room temperature. The thickness of the films was measured using ImageJ.

1.4 Conclusion

In conclusion, fully negative-charged (FNC) LbL nanofilms were fabricated using the CuAAC click reaction. The nanofilm fabrication strategy overcomes the electrostatic repulsion between negative-charged PAA. The fabricated nanofilms contain high-density free carboxyl groups, which are sensitive to pH variations. Under treatment with different pH solutions, the carboxyl groups respond rapidly to be protonated or deprotonated and instantly result in the shrinking or swelling of the nanofilm. Notably, the swelling ratio of the nanofilms is dependent on the charge density, which is controlled by the graft degree of functionalized PAA. Since all the individual layers are covalently bonded to each other, the obtained LbL nanofilms are very stable under harsh pH conditions. The pH-induced thickness change was shown to be repeatable without affecting the nanofilm's stability. This work suggests a highly effective method of fabricating FNC LbL nanofilms with tunable thickness and charge density.

The fully single-charged LbL nanofilm fabrication strategy allows for the assembly of different PE with the same kind of charge. For example, two different polyanions could potentially be used to make the composite backbone. The choice of polymer is also not limited to negative-charged polymers, as there exists a large number of polycations, and the electrostatic repulsion between them can be reduced by increasing the assembly pH value. The introduction of new interactions is the key point of the present method. In view of its LbL assembly principle, the proposed strategy is believed to be generally applicable.

1.5 Reference

[1] G. K. Such, E. Tjipto, A. Postma, A. P. R. Johnston, F. Caruso, *Nano Lett.* **2007**, *7*, 1706.

[2] C. R. Kinnane, G. K. Such, F. Caruso, *Macromolecules* **2011**, *44*, 1194.

[3] G. K. Such, J. F. Quinn, A. Quinn, E. Tjipto, F. Caruso, *J. Am. Chem. Soc.* **2006**, *128*, 9318.

[4] C. J. Ochs, G. K. Such, B. Städler, F. Caruso, *Biomacromolecules* **2008**, *9*, 3389.

[5] H. C. Kolb, M. G. Finn, K. B. Sharpless, *Angew. Chem. Int. Ed.* **2001**, *40*, 2004.

[6] S. Liu, Y. Cao, Z. Wu, H. Chen, *J. Mater. Chem. B* **2020**, *8*, 5529.

[7] C. Schulz, S. Nowak, R. Fröhlich, B. J. Ravoo, *Small* **2012**, *8*, 569.

[8] Y. Li, D. Wang, J. M. Buriak, *Langmuir* **2010**, *26*, 1232.

[9] F. Yu, X. Cao, L. Zeng, Q. Zhang, X. Chen, *Carbohydr. Polym.* **2013**, *97*, 188.

[10] J. M. Pelet, D. Putnam, *Bioconjug. Chem.* **2011**, *22*, 329.

[11] F. Yu, X. Cao, Y. Li, L. Zeng, B. Yuan, X. Chen, *Polym. Chem.* **2013**, *5*, 1082.

[12] K. Kadowaki, M. Matsusaki, M. Akashi, *Langmuir* **2010**, *26*, 5670.

[13] Y. Lvov, K. Ariga, I. Ichinose, T. Kunitake, *J. Am. Chem. Soc.* **1995**, *117*, 6117.

[14] A. Nebbioso, P. Mazzei, *Magn. Reson. Chem.* **2016**, *54*, 937.

[15] L. B. Sagle, Y. Zhang, V. A. Litosh, X. Chen, Y. Cho, P. S. Cremer, *J. Am. Chem. Soc.* **2009**, *131*, 9304.

[16] T. Guckeisen, S. Hosseinpour, W. Peukert, *J. Colloid Interface Sci.* **2021**, *590*, 38.

[17] R. Lu, X. Zhang, X. Cheng, X. Zan, W. Geng, *Langmuir* **2021**, *37*, 13000.

[18] Y. Min, P. T. Hammond, *Chem. Mater.* **2011**, *23*, 5349.

[19] V. Selin, J. F. Ankner, S. A. Sukhishvili, *Macromolecules* **2015**, *48*, 3983.

[20] D. A. Roberts, B. S. Pilgrim, T. N. Dell, M. M. Stevens, *Chem. Sci.* **2020**, *11*, 3713.

[21] F. Hegaard, E. Thormann, *Langmuir* **2023**, *39*, 5012.

[22] A. Nolte, S. Hossfeld, B. Schroeppel, A. Mueller, D. Stoll, T. Walker, H. P. Wendel, R. Krastev, *J. Biomater. Appl.* **2013**, *28*, 84.

[23] A. Jafari, H. Sun, B. Sun, M. Alaa Mohamed, H. Cui, C. Cheng, *Chem. Commun.* **2019**, *55*, 1267.

[24] G. Kocak, C. Tuncer, V. Bütün, *Polym. Chem.* **2017**, *8*, 144.

[25] G. Sauerbrey, *Z. Für Phys.* **1959**, *155*, 206.

[26] M. Todica, R. Stefan, C. V. Pop, L. Olar, *Acta Phys. Pol. A* **2015**, *128*, 128.

[27] D. G. Mintis, V. G. Mavrantzas, *J. Phys. Chem. B* **2019**, *123*, 4204.

[28] X. Hou, F. Li, Y. Song, M. Li, *J. Phys. Chem. Lett.* **2022**, *13*, 2885.

[29] V. Hwang, A. B. Stephenson, S. Barkley, S. Brandt, M. Xiao, J. Aizenberg, V. N. Manoharan, *Proc. Natl. Acad. Sci.* **2021**, *118*, e2015551118.

[30] F. Meng, B. Ju, Z. Wang, R. Han, Y. Zhang, S. Zhang, P. Wu, B. Tang, *J. Am. Chem. Soc.* **2022**, *144*, 7610.

[31] J. Xue, X. Yin, L. Xue, C. Zhang, S. Dong, L. Yang, Y. Fang, Y. Li, L. Li, J. Cui, *Nat. Commun.* **2022**, *13*, 7823.

[32] H. Zhang, J. Guo, Y. Wang, L. Sun, Y. Zhao, *Adv. Sci.* **2021**, *8*, 2102156.

Chapter 2 Fabrication of fully positively-charged LbL nanofilms

2.1 Introduction

Previous chapter demonstrated the fabrication of fully negatively charged (FNC) LbL nanofilms using azide and alkyne functionalized poly (acrylic acid) (PAA). The film assembly was driven by CuAAC reaction. Because of the high charge density, the FNC films were sensitive to pH changes and showed pH-induced thickness and surface morphology transition.[1] In this study, we expanded the film fabrication strategy to prepare a fully-positively charged (FPC) LbL nanofilm. As shown in **Figure 2-1a**, LbL nanofilms with positive charges spread over the entire films were prepared using CuAAC reaction. Poly-L-lysine (PLL) was partially functionalized with azide and alkyne groups. Due to the high reactivity of azide and alkyne groups, LbL nanofilms can be fabricated with the presence of Cu(I) as a catalyst. To overcome the electrostatic repulsion between amino groups along PLL, our strategy was to assemble at a higher pH to deprotonate amino groups therein, thereby reducing the electrostatic repulsion of the PLL backbone. After the formation of stable triazole, the ionization degree of amino groups could be tuned by adjusting the pH, while the conventional PE LbL nanofilms dissociated in harsh pH environments (**Figure 2-1b**). Owing to the high charge density, this kind of LbL nanofilm shows pH responsiveness and good adsorption properties (**Figure 2-1b c**).

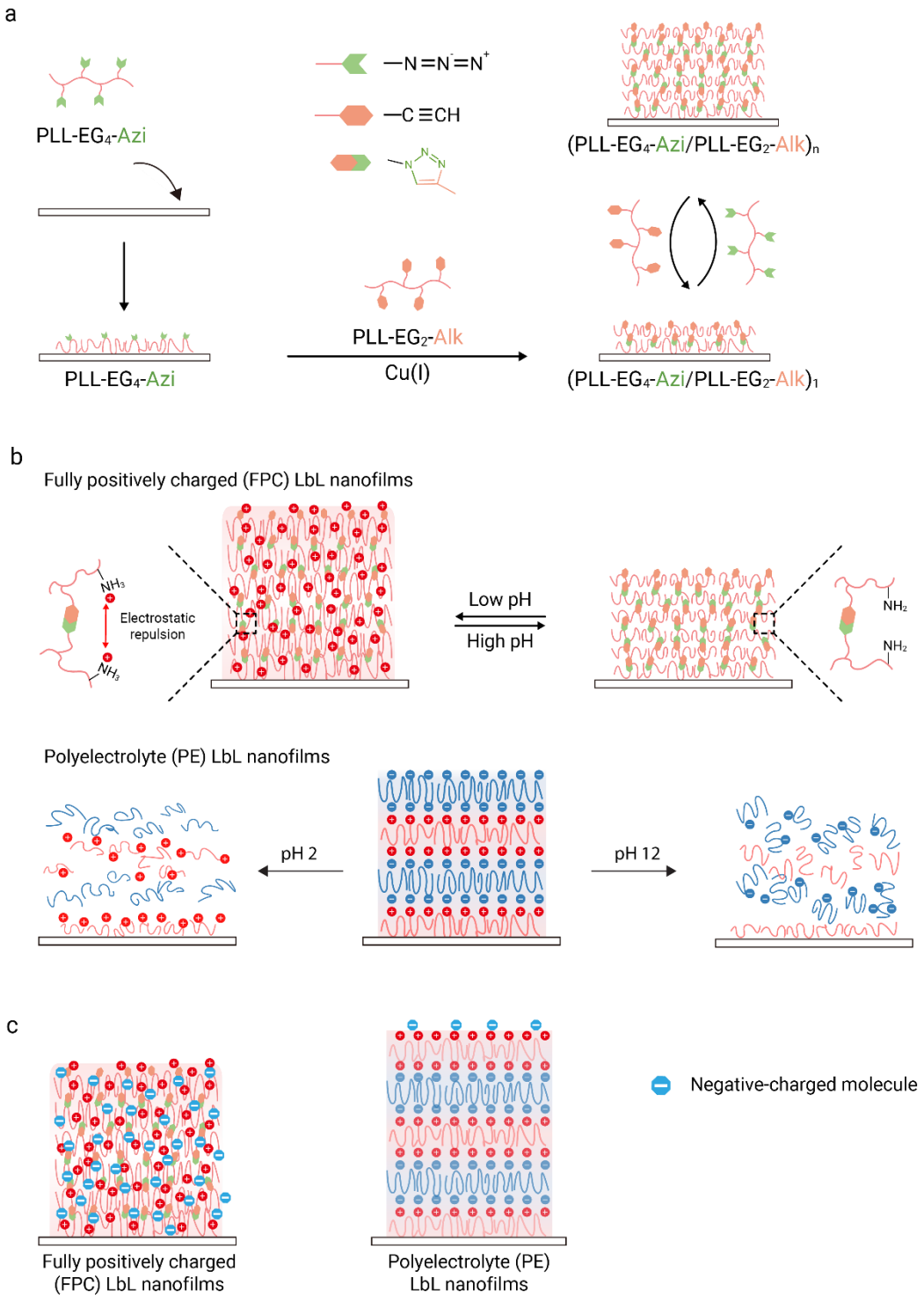

Figure 2-1 (a) Schematic illustration of FPC LbL nanofilm fabrication via click reaction. (b) Upper: pH-induced swelling and shrinking behavior of FPC LbL nanofilms; Lower: pH-induced dissociation behavior of PE LbL nanofilms. (c) Comparison of the adsorption properties between FPC LbL nanofilms and polyelectrolyte LbL nanofilms.

2.2 Experiment

2.2.1 Materials

Poly-L-lysine hydrobromide (PLL, 15-30 kDa), Copper (II) sulfate pentahydrate ($CuSO_4 \cdot 5H_2O$), sodium L-ascorbate ($C_5H_7NaO_6$), Azido-dEG®$_4$-acid (Azi-EG$_4$-acid, >90%), and deuterium chloride solution (35 wt% in D_2O, >99 atom % D) were purchased from Sigma-Aldrich. Poly (acrylic acid) (PAA, 25 kDa), sodium carbonate ($NaCO_3$, 99.8%), sodium hydroxide (NaOH, 93.0%), hydrochloric acid (HCl, 5M), sulfuric acid (H_2SO_4, 95.0%), and ethylenediaminetetraacetic acid disodium salt dihydrate (EDTA) were purchased from Wako Pure Chemical Industries. Sodium hydrogen carbonate was purchased from Nacalai Tesque, INC. 4-(4,6-Dimethoxy-1,3,5-triazin-2-yl)-4-methyl morpholinium chloride (DMTMM, 97.5%) was purchased from Watanabe. Hydrogen peroxide (H_2O_2, 35%) was purchased from Kishida Chemical Co., Ltd. Propargyl-EG$_2$-acid (Alk-EG$_2$-acid, 98%) was purchased from BroadPharm. Deuterium oxide (D_2O, 99.9%), and sodium deuteroxide (D, 99.5%, 40% in D_2O) were purchased from Cambridge Isotope Laboratories, Inc.

2.2.2 Synthesis of PLL-EG$_4$-Azi

Azide modified PLL was synthesized via DMTMM-mediated conjugation. Briefly, PLL (60 mg, 0.47 mmol) was dissolved in 10 mL of bicarbonate buffer solution (pH 8.5, 0.1 M), to which DMTMM was added and stirred for 10 min. Azi-EG$_4$-acid in a 0.1 (13.63 mg, 0.047 mmol), 0.25 (34.09 mg, 0.117 mmol), and 0.5 (68.17 mg, 0.234 mmol) molar ratio (relative to the -NH_2 groups in PLL) was dissolved in 10 mL bicarbonate buffer solution (pH 8.5, 0.1 M). The solution was then added dropwise to the PLL solution. The reaction was conducted at room temperature for 24 h and the solution was then dialyzed against Milli-Q water for 3 days (MWCO: 3500 Da). After dialysis, PLL-EG$_4$-Azi was obtained by lyophilization.

2.2.3 Synthesis of PLL-EG$_2$-Alk

PLL functionalized with alkynes was also prepared via DMTMM conjugation in Milli-Q water. Briefly, PLL (60 mg, 0.47 mmol) was dissolved in 10 mL of Milli-Q water. After completely dissolving, DMTMM was added to the PLL solutions. Alk-EG$_2$-acid in a 0.1 (8.06 mg, 0.047 mmol), 0.25 (20.15 mg, 0.117 mmol), and 0.5 (40.30 mg, 0.234 mmol) molar ratio (relative to the -NH_2 groups in PLL) was dissolved in 10 mL of Milli-Q water and added dropwise to the PLL solution. The pH was adjusted to 5.5 using 0.1 M NaOH. The reaction was conducted at room temperature for 24 h. The PAA-EG$_2$-Alk was purified by dialysis

(MWCO: 3500 Da) against Milli-Q water for 3 days and lyophilized.

2.2.4 Click reaction monitoring using ^{1}H-NMR

For CuAAC reaction monitoring, $CuSO_4$ (0.6 mg/mL) and sodium ascorbate (SA, 1.46 mg/mL) were dissolved in D_2O. The pH of all the solutions including D_2O were adjusted to 5.5 using deuterium chloride solution or sodium deuteroxide. Fresh Cu(I) solution was prepared by mixing $CuSO_4$ solution, SA solution, and D_2O at a volume ratio of 1:1:3. PLL-EG_4-Azi and PLL-EG_2-Alk were dissolved in a freshly prepared Cu(I) solution to obtain a solution with a concentration of 3.2 mg/mL, then 0.4 mL of each polymer solution was transferred to a 5 mm NMR-tube with a polymer concentration of 1.6 mg/mL. ^{1}H-NMR spectra were obtained at 30 min intervals over 17 h.

2.2.5 Fabrication of fully-positively charged (FPC) layer-by-layer (LbL) nanofilm

Layer-by-layer nanofilm fabrication was monitored by quartz crystal microbalance (QCM) (AFFINIX Q8, 27 MHz, ULVAC). QCM sensors with a gold coating (QCM01S, ULVAC) were used as a substrate. QCM sensors were treated with 5 μL piranha solution (H_2SO_4: 35% H_2O_2 = 3:1) for 10 min and repeated 3 times. 100 μL of Cu(I) solution (pH 5.5, 0.36 mg/mL $CuSO_4$, 0.88 mg/mL SA) was added into the cells until the frequency stabilized. 5 μL of PLL-EG_4-Azi solution was injected into the cells. The frequency changes along the polymer solution injection were recorded by the QCM. After 15 min of incubation, the QCM sensors were rinsed with 100 μL Milli-Q water (pH 5.5) 3 times and reached a frequency equilibration in 100 μL of Cu(I) solution. 5 μL of PLL-EG_2-Alk solutions were injected into the cells for the deposition of the second layer. By altering the polymer solutions in the cells, nanofilms could be fabricated layer-by-layer via the click reaction until they were assembled to the desired number of layers. EDTA (0.02 M) solutions were used to wash the copper ions away by forming an EDTA-Cu complexation.[2,3]

The polymer mass (Δm) that was deposited on the QCM sensor was calculated with the Sauerbrey equation. A frequency change of 1 Hz corresponded to a mass change of 0.62 ng/cm^2 in the QCM system used here (eq. 2-1).

$$-\Delta m(\mathrm{ng}\ /\ \mathrm{cm}^2) = 0.62\Delta F(\mathrm{Hz}) \qquad (2-1)$$

After further calculation according to the deposited amount and assumed nanofilm density of the polyelectrolyte at 1.2 g/cm^3,[4,5] the thickness of the fabricated nanofilms was

calculated via the following equation (eq. 2-2):

$$Thickness\ (\mathrm{nm}) = \frac{\Delta m(\mathrm{ng}\ /\ \mathrm{cm}^2)}{1.2 \times 10^9(\mathrm{ng}\ /\ \mathrm{cm}^3)} \times 10^7 \qquad (2-2)$$

2.2.6 Characterization of pH responsive properties

The pH-responsiveness of the FPC LbL nanofilms was also evaluated by the QCM. After fabrication, the nanofilms were incubated in 100 μL solutions with different pH values. The swelling ratio of the nanofilms from pH 2 to pH 12 was calculated according to the following equation (eq. 2-3):

$$\text{Swelling ratio}\ (\%) = \frac{Th_2}{TH_{12}} \times 100\% \qquad (2-3)$$

Where Th_2 and Th_{12} represent the thickness of nanofilms at pH 2 and pH 12, respectively.

2.2.7 Adsorption experiments

The adsorption properties of FPC LbL nanofilms were measured by QCM using Eosin-Y as the model negative-charged molecules. After the fabrication of the LbL nanofilms, they were incubated in Eosin-Y solutions until frequency equilibration. The frequency shifts were recorded and calculated according to eq. 1. The images of QCM sensor after adsorption were captured using fluorescent microscopy (Olympus MVX10, Tokyo, Japan)

2.2.8 AFM observation

Layer-by-layer nanofilms were fabricated on silicon wafers via standard dip assembly protocols. The silicon wafers were treated with plasma for 10 min, then alternately dipped in PLL-EG_2-Azi and PLL-EG_2-Alk solutions containing Cu(I). Between each step, the silicon wafers were rinsed with Milli-Q water (pH 5.5).

2.2.9 Characterization methods

The chemical structure of the functionalized polymers was analyzed by ^{1}H-NMR (Jeol, JNM-GSX 400, Japan).

2.3 Results and discussions

2.3.1 Synthesis of PLL-EG$_4$-Azi and PLL-EG$_2$-Alk

Both PLL-EG$_4$-Azi and PLL-EG$_2$-Alk were synthesized by grafting azide and alkyne groups to the PLL via amide bond formation between the amino groups of the lysine side chains and carboxyl groups of azi-EG$_4$-acid and alk-EG$_2$-acid, respectively (**Figure 2-2a** and **Figure 2-3a**). ^{1}H-NMR spectra confirmed the structure of the obtained polymers. For PLL-EG$_4$-Azi, as shown in **Figure 2-2b**, the peaks observed in the range of 3.9-3.6 ppm corresponded to the methylene next to oxygen while the peak at 3.53 ppm represented the methylene next to the azide group. Furthermore, after azide modification, the peak at 3.05 ppm split into two peaks due to the partial amidation of amino groups at the side chains of PLL. By varying the feeding ratio, we successfully synthesized PLL-EG$_4$-Azi with different graft ratios (**Figure 2-2c**). Similarly, in **Figure 2-3b**, for alkyne modified PLL, the peaks observed in the range of 3.81-3.69 ppm corresponding to the methylene of the side chains. Peaks at 4.25 ppm and 2.48 ppm were attributed to the proton next to alkyne groups and C=O bond, respectively. To distinguish PLL with different graft ratios, functionalized polymers were named by their graft ratio as a subscript. For azide modified PLL, they were named PLL-EG$_4$-Azi$_{09}$, PLL-EG$_4$-Azi$_{21}$, and PLL-EG$_4$-Azi$_{48}$ (**Figure 2-2c**). For alkyne-modified PLL, they were named PLL-EG$_2$-Alk$_6$, PLL-EG$_2$-Alk$_{15}$, and PLL-EG$_2$-Alk$_{44}$ (**Figure 2-3c**).

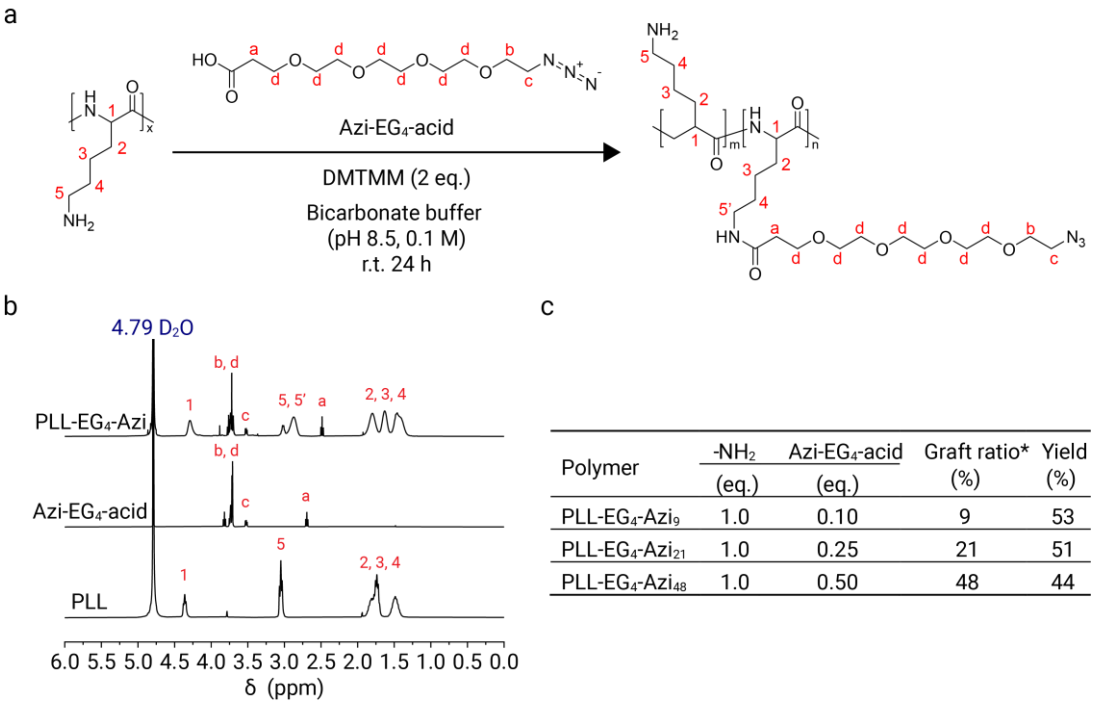

Polymer	-NH$_2$ (eq.)	Azi-EG$_4$-acid (eq.)	Graft ratio* (%)	Yield (%)
PLL-EG$_4$-Azi$_9$	1.0	0.10	9	53
PLL-EG$_4$-Azi$_{21}$	1.0	0.25	21	51
PLL-EG$_4$-Azi$_{48}$	1.0	0.50	48	44

Figure 2-2 (a) Synthesis of PLL-EG4-Azi. (b) ^{1}H-NMR spectra of PLL, Azi-EG4-acid, and PLL-EG4-Azi. (c) Feeding ratio and graft ratio of PLL-EG4-Azi.

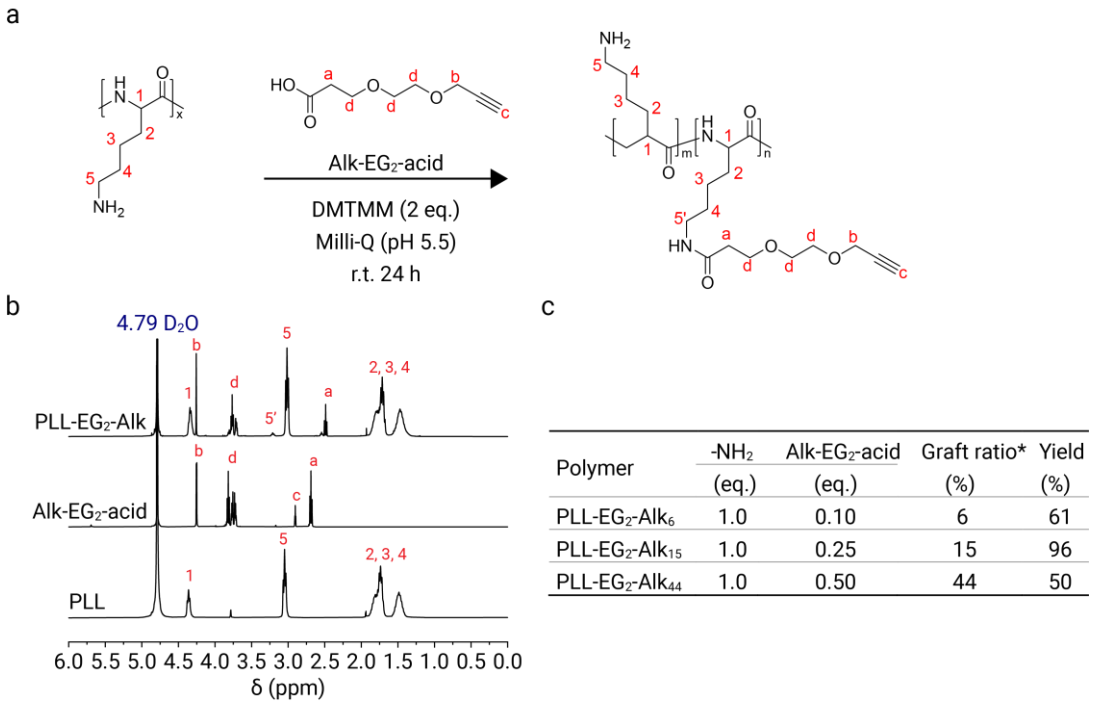

Polymer	-NH_2 (eq.)	Alk-EG_2-acid (eq.)	Graft ratio* (%)	Yield (%)
PLL-EG_2-Alk_6	1.0	0.10	6	61
PLL-EG_2-Alk_{15}	1.0	0.25	15	96
PLL-EG_2-Alk_{44}	1.0	0.50	44	50

Figure 2-3 (a) Synthesis of PLL-EG4-Azi. (b) ^{1}H-NMR spectra of PLL, Alk-EG2-acid, and PLL-EG2-Alk. (c) Feeding ratio and graft ratio of PLL-EG2-Alk.

2.3.2 Real-time click reaction Monitoring

The real-time click reaction was monitored by measuring ^{1}H-NMR spectra. As shown in **Figure 2-4a**, the reaction was initiated by administering the Cu(I) catalyst to the solution containing both PLL-EG4-Azi and PLL-EG2-Alk.

The click chemistry reaction was determined by evaluating the integral of selected proton signals aiming to monitor the consumption of reagents (*q*: -C***H*****$_2$**-N_3) and the formation of triazole (peaks *o* and *p*). The first evidence of the reaction occurrence was the immediate quenching of the methylene proton signal next to alkyne groups at 4.25 ppm due to the rapid complexation with Cu(I)[6] (**Figure 2-4b**). Furthermore, the conversion of the azide groups led to a decrease in intensity of -C***H*****$_2$**-N_3 (peak *q*), and the appearance of new proton signals which were assigned to the adjoining protons next to the triazole rings[7] (*o* and *p*) (**Figure 2-4b**). The reagents' peaks showed a decreasing trend over reaction time, while the triazole's peaks displayed the opposite behavior (**Figure 2-4c**). The consumption of -C***H*****$_2$**-N_3 was

calculated according to the decreasing portion of peak integral and the result showed that 50.5% of azide groups were reacted.

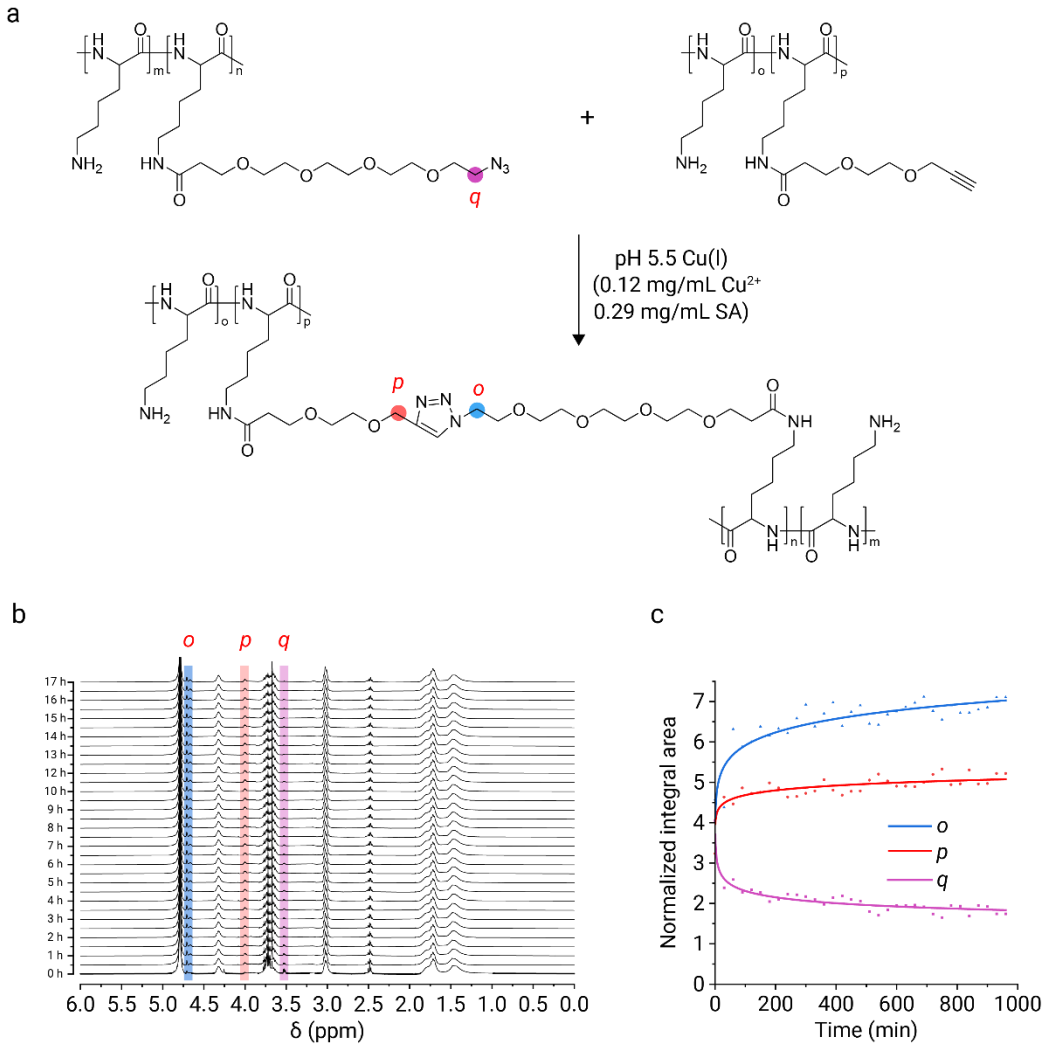

Figure 2-4 ^{1}H-NMR spectra of real-time monitoring of the click reaction. (a) Formation of triazole by the click reaction between PLL-EG$_4$-Azi and PLL-EG$_2$-Alk with the presence of Cu(I). Cu(I) solution contains 0.12 mg/mL of $CuSO_4$ and 0.29 mg/mL of SA. (b) ^{1}H-NMR stacked plot of the CuAAC reaction with the presence of Cu(I). Spectra were taken every 30 min. (c) Normalized integrals of the -C$\boldsymbol{H_2}$-N$_3$ (peak *q*, violet) and protons adjoining to triazole rings (peaks *o* and *p*, blue and red) over reaction time.

2.3.3 Fabrication of fully-positively charged (FPC) layer-by-layer (LbL) nanofilms

As shown in **Figure 2-1a**, the FPC LbL nanofilms were fabricated by alternately exposing the substrate to PLL-EG$_4$-Azi and PLL-EG$_2$-Alk. With Cu(I) in the solutions, the copper-catalyzed click reaction (CuAAC) was conducted between azide and alkyne groups

and formed the triazole ring, leading to the absorption of polymer to the pre-layer. The LbL assembly of the nanofilms was monitored by quartz crystal microbalance (QCM), starting with the more hydrophilic PLL-EG_4-Azi followed by the addition of PLL-EG_2-Alk. As shown in **Figure 2-5a**, every time the polymers were added, a frequency decrease was observed due to the adsorption of PLL-EG_4-Azi or PLL-EG_2-Alk. After 15 min, the frequency stabilized, indicating that the adsorption of polymers reached saturation. Then the sensors were rinsed with pH 5.5 Milli-Q water, at which point the frequency increased indicating the washing away of some weakly attached polymers. After the nanofilm assembly, the EDTA washing step markedly increased the frequency, indicating the washing away of copper ions remaining in the nanofilms.[2,3]

Theoretically, a higher pH reduces the electrostatic interactions between PLL chains. As shown in **Figure 2-6**, compared with the marked stepwise thickness increase observed from the nanofilm assembled at pH 5.5, nanofilms could barely assemble at pH 3.5. To facilitate the LbL assembly, the pH of all solutions was adjusted to 5.5 to partially deprotonate the PLL and reduce the electrostatic repulsion between polymer chains.

The graft ratio of functional groups also affects the thickness of the nanofilms. **Figure 2-5b** shows the negative frequency shift ($-\Delta F$) at each assembly step and the EDTA washing step. After EDTA washing, thicker films were observed with an increasing graft ratio, and the film thickness increased from 24 to 39 nm (**Figure 2-5c**). Thicker films can be attributed to a stronger driving force due to more reaction moieties for click reaction along polymer chains with a higher graft ratio. Another feature of the FPC LbL nanofilms was the linear growth thickness for layer, indicating the steady deposition of polymers, which is different from the non-linear growth for most polyelectrolyte LbL nanofilms at a fixed deposition time.[8,9]

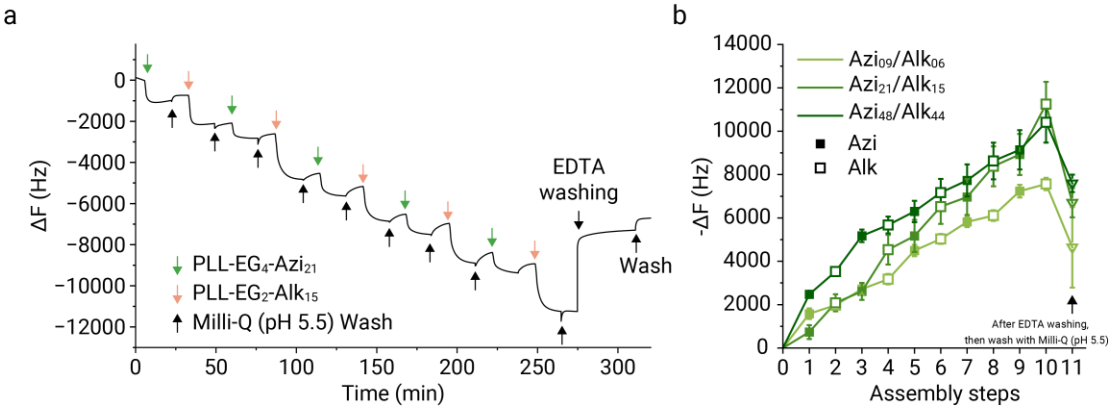

c

	Before EDTA washing			After EDTA washing		
	Frequency (Hz)	Mass (ng/cm²)	Thickness (nm)	Frequency (Hz)	Mass (ng/cm²)	Thickness (nm)
Azi_{09}/Alk_{06}	-7564	4690	39	-4643	2879	24
Azi_{21}/Alk_{15}	-11250	6975	58	-6702	4155	35
Azi_{48}/Alk_{44}	-10409	6454	54	-7596	4710	39

Figure 2-5 Analysis of the LbL assembly process by QCM. (a) Frequency shifts (ΔF) plotted against time for a $(PLL\text{-}EG_4\text{-}Azi_{21}/PLL\text{-}EG_2\text{-}Alk_{15})_5$ LbL nanofilm assembly with a polymer concentration of 0.16 mg/mL. Vertical arrows indicate the moment of adding polymer solutions to the QCM cell and the start of rinsing steps using Milli-Q water (pH 5.5) or EDTA solutions. (b) Frequency shift of a $(PLL\text{-}EG_4\text{-}Azi/PLL\text{-}EG_2\text{-}Alk)_5$ LbL nanofilm assembled by functionalized PLL with different graft ratios at each step (n > 3). The concentration of all the polymer solutions was 0.16 mg/mL. (c) The frequency shift, corresponding to the absorbed polymer mass and thickness of the LbL nanofilm before and after EDTA washing.

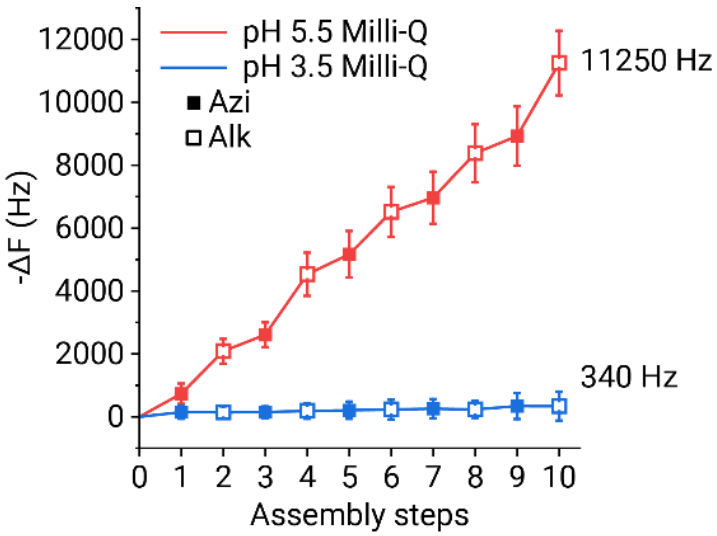

Figure 2-6 Frequency shift of (PLL-EG$_4$-Azi$_{21}$/PLL-EG$_2$-Alk$_{15}$)$_5$ LbL nanofilms assembled at different pH. The concentration of all the polymer solutions was 0.16 mg/mL

AFM images confirmed the EDTA washing step led to the decrease in nanofilm thickness. As shown in **Figure 2-7**, the height profile across the scratched edge of the nanofilms showed the thickness of nanofilms decreased from 43 nm (**Figure 2-7b**) to 26 m (**Figure 2-7d**). The thickness measured by AFM was thinner than that from the QCM, which were 58 nm and 35 nm before and after EDTA washing, respectively. But the QCM measured the nanofilms in liquid while AFM measurement was performed after the nanofilms were dried. The thickness decrease might be attributed to the loss of water. We hypothesized that the EDTA washing removed the remaining copper ions in the nanofilms by forming a Cu-EDTA complexation,[2,3] so the thickness decreased. Additionally, the EDTA washing step led to a more homogeneous nanofilm, which was indicated by the decrease of the surface roughness (Ra) from 35 nm to 12 nm after EDTA washing.

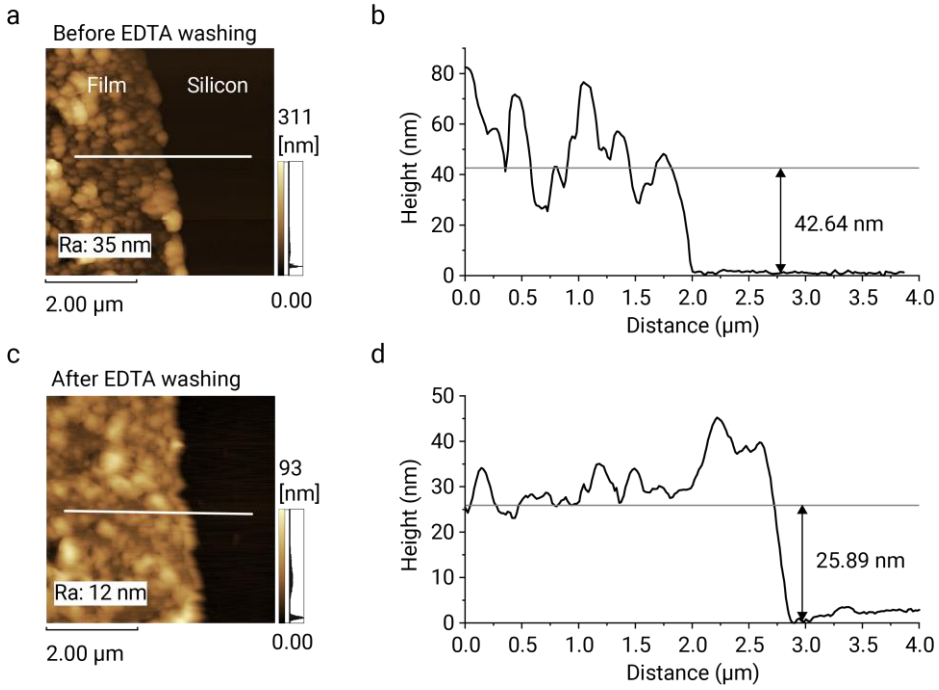

Figure 2-7 AFM height images of a (PLL-EG$_4$-Azi$_{21}$/PLL-EG$_2$-Alk$_{15}$)$_5$ LbL nanofilm before (a) and after (c) EDTA washing (inserted is the surface roughness (Ra) measured via the AFM). The height profile lines reveal the thickness of the nanofilm before (b) and after (d) EDTA washing

2.3.4 pH-induced thickness changing of FPC LbL nanofilms

The LbL nanofilms fabricated in this study contained a large number of amino groups along the PLL chains, which were able to gain a positive charge at a low pH and lose the charge at a high pH. The differing state of the polymer backbone affected the properties of nanofilms. Herein, we investigated how the pH affects the nanofilms properties using QCM. After nanofilm fabrication on the QCM sensors, they were incubated in Milli-Q water with differing pH values, and the corresponding frequency was recorded. In this study, to ensure the consistent ionic strength and observe the maximum thickness change for the swelling ratio calculation. nanofilms were incubated in the pH 12 and pH 2 solutions that adjusted using NaOH and HCl, respectively, maintaining the same ionic strength of 0.01 mol/L. As shown in **Figure 2-8a**, all the films showed repeatable pH-induced thickness change behavior. For the nanofilms fabricated by the polymers with low (Azi_{09}/Alk_{06}) and medium (Azi_{21}/Alk_{15}) graft degrees, the nanofilms swelled at a low pH but shrank at a high pH, but for the nanofilms fabricated by high graft ratio (Azi_{48}/Alk_{44}) polymers, they showed an opposite thickness change, i.e., swelling at a high pH but shrinking at a low pH. The swelling and shrinking of the nanofilms can be associated with the protonation and deprotonation of the amino groups along the PLL polymer backbone. For nanofilms with low and medium functional groups, a low pH resulted in the protonation of amino groups that generated electrostatic repulsion, making the nanofilms swell. At a high pH, the amino groups in the nanofilms lost the charges and the electrostatic repulsion disappeared, thus the swollen nanofilms shrank (**Figure 2-8b**). Nanofilms with a high graft ratio of functional groups showed the opposite trend possibly because the amount of free amino groups was the lowest, so the nanofilms were not sensitive. Additionally, for nanofilms with higher graft ratio, after the deprotonation of amine groups, the osmotic pressure caused by the polymer-water interaction draws more solutions into the nanofilms, leading to swelling instead.[10,11] It is noteworthy that the swelling-shrinking of the nanofilms was repeatable, indicating the stability of FPC LbL nanofilms compared with polyelectrolyte (PE) LbL nanofilms. As shown in Figure S10, after incubating $(PLL\text{-}EG_4\text{-}Azi_{21}/PLL\text{-}EG_2\text{-}Alk_{15})_5$ and $(PLL/PAA)_5$ PE LbL nanofilms at pH 2 and pH 12, the PE nanofilms dissociated rapidly at both pH conditions. Meanwhile, the FPC LbL nanofilms were stable for over 13 h in a harsh pH environment, which was mainly attributed to the triazole rings between $PLL\text{-}EG_4$-Azi and $PLL\text{-}EG_2$-Alk.[12]

To quantify the pH response sensitivity, the swelling ratio of different LbL nanofilms was calculated via the thickness of nanofilms at different pHs. As shown in **Figure 2-8c** and

Figure 2-8d, as the graft ratio of PLL increased, the swelling ratios of the corresponding nanofilms were 158, 108 and 92%. Greater thickness changes were observed with a lower graft ratio and this lower ratio yielded more free amino groups, resulting in a stronger electrostatic repulsion in the nanofilms. Some of the polymers may also detached from the nanofilms due to the stronger electrostatic repulsion, making there is a slight decreasing of thickness of nanofilms with low graft ratio. Additionally, the nanofilms with a lower graft ratio had a lower crosslinking degree, making the network of the nanofilms less dense.

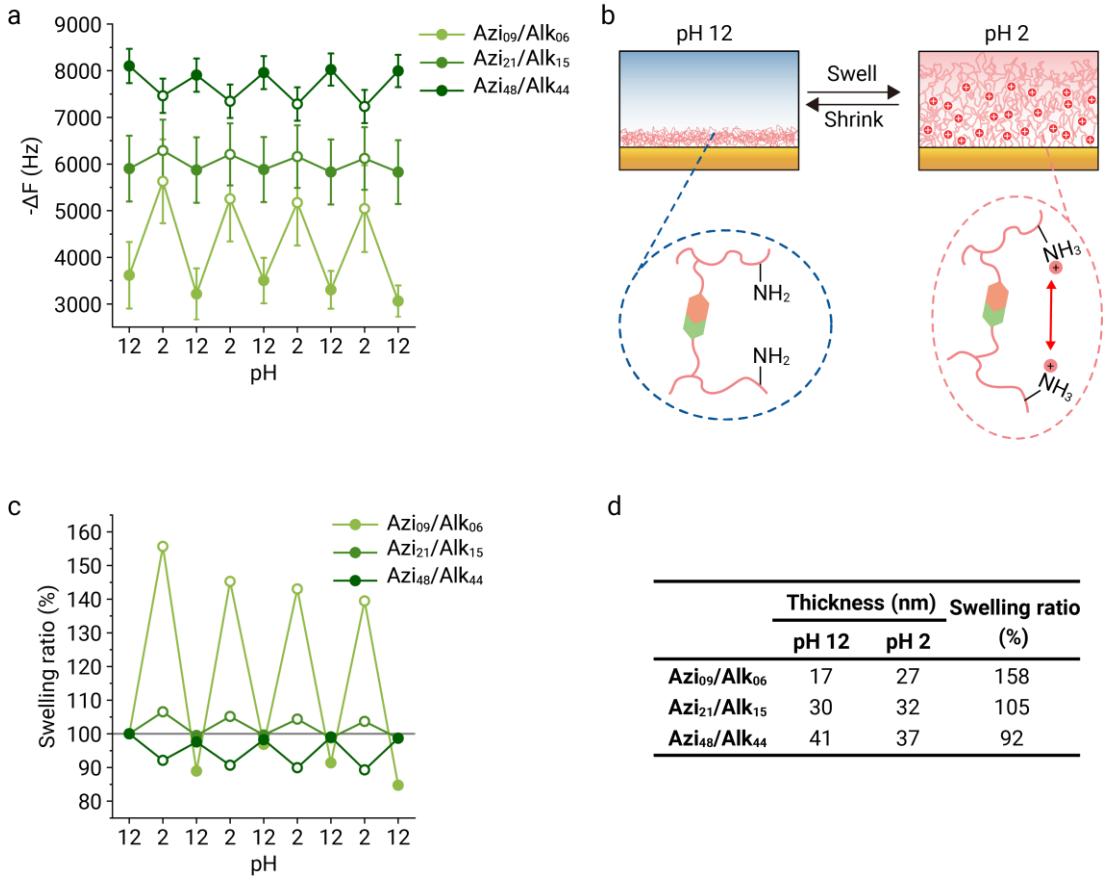

	Thickness (nm)		Swelling ratio (%)
	pH 12	pH 2	
Azi_{09}/Alk_{06}	17	27	158
Azi_{21}/Alk_{15}	30	32	105
Azi_{48}/Alk_{44}	41	37	92

Figure 2-8 pH-induced thickness and morphology change of FPC LbL nanofilms. (a) Thickness change of $(PLL\text{-}EG_4\text{-}Azi/PLL\text{-}EG_2\text{-}Alk)_5$ LbL nanofilms at pH 2 and pH 12. (b) Schematic depicting the swelling and shrinking of FPC LbL nanofilms. (c) Swelling ratio of $(PLL\text{-}EG_4\text{-}Azi/PLL\text{-}EG_2\text{-}Alk)_5$ LbL nanofilms from pH 12 to 2. (d) Thickness and swelling ratio of $(PLL\text{-}EG_4\text{-}Azi/PLL\text{-}EG_2\text{-}Alk)_5$ LbL nanofilms fabricated with different graft degrees. The concentrations of all polymer solutions were 0.16 mg/mL.

To further investigate the more detailed pH -dependent thickness change of FPC LbL nanofilms, they were incubated in the solutions of different pH between pH 2 and 12. As

shown in **Figure 2-9**, when the pH increased from 2 to 9, the thickness of the nanofilms kept steady. However, when the pH exceeded 9, the thickness the thickness decreased significantly. This phenomenon is attributed to the protonation and deprotonation of the amino groups along the PLL polymer backbone. pH higher than 9 results in the deprotonation of amino groups, then eliminate the electrostatic repulsion and make the nanofilms shrink. This observation is consistent with the pKa of PLL which is around 9.[13]

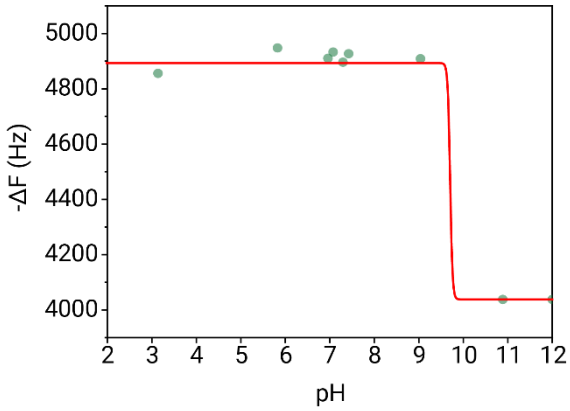

Figure 2-9 Relationship between the thickness of (PLL-EG$_4$-Azi$_{09}$/PLL-EG$_2$-Alk$_{06}$)$_5$ LbL nanofilms and pH values from 2 to 12.

To further investigate how the pH affects the properties of FPC LbL nanofilms, AFM measurements were taken when the (PLL-EG$_4$-Azi$_{21}$/PLL-EG$_2$-Alk$_{15}$)$_5$ LbL nanofilms were incubated in pH 12 and pH 2 solutions. As shown in **Figure 2-10**, a higher pH led to the increasing of surface roughness (Ra) from 4.6 nm (**Figure 2-10a**) to 15 nm (**Figure 2-10c**). In agreement with the protonation and deprotonation of amino groups at different pHs, nanofilms at a low pH tended to be more swollen because of the electrostatic repulsion. At a high pH, deprotonation of amino groups resulted in the disappearance of interpolymer repulsion, forming the agglomerate surface morphology. According to the height profiles, the thickness of the nanofilm in pH 12 was 32 nm (**Figure 2-10b**), much thinner than the 104 nm (**Figure 2-10d**) in pH 2 solutions. The thickness difference indicates pH-induced shrinking and swelling behavior of the nanofilms due to the pH-dependent ionization of amino groups. In pH 12 solutions, the results of AFM measurement matched the results of QCM measurement. However, in pH 2 solutions, the thickness obtained from AFM was 104 nm, much thicker than that from QCM. The difference between these two measurements may be because the thickness measured from the QCM was calculated with an assumed polymer density of 1.2 g/cm^3, but the nanofilms were in a swollen state in pH 2 solutions, so the actual

density of the nanofilms should be lower because of water absorption.

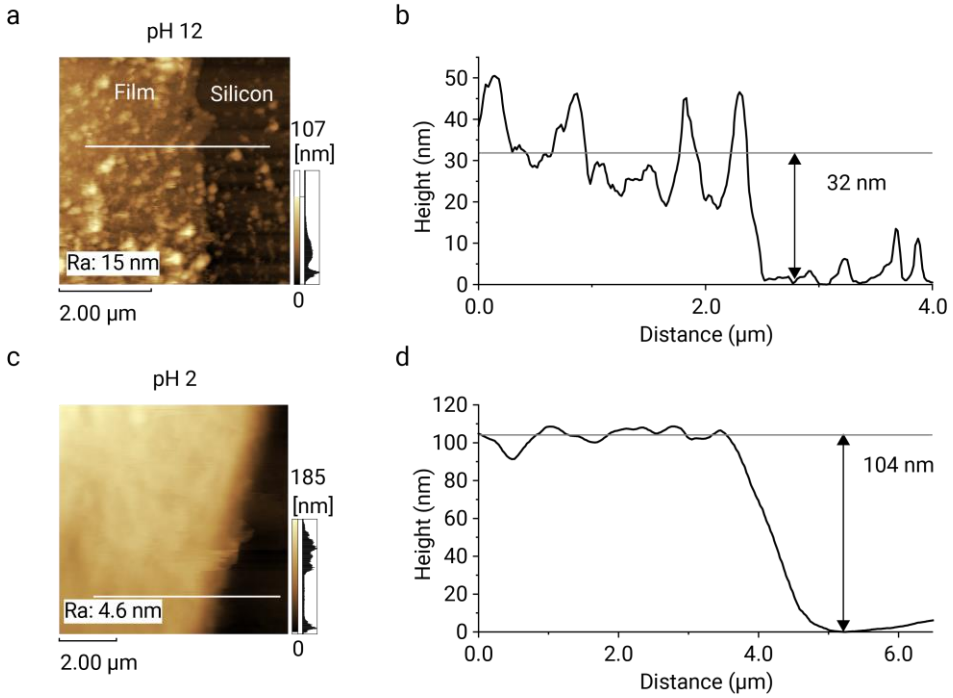

Figure 2-10 AFM height images of (PLL-EG_4-Azi_{21}/PLL-EG_2-Alk_{15})$_5$ LbL nanofilms in the solutions of pH 12 (a) and pH 2 (c) (inserted is the surface roughness (Ra) measured by AFM). The height profile lines reveal the thickness of the nanofilms in the solutions of pH 12 (b) and pH 2 (d). The concentrations of all polymer solutions were 0.16 mg/mL.

2.3.5 Adsorption properties of FPC LbL nanofilms

Due to the structure of the LbL nanofilms, there is an abundance of amino groups giving the films a high charge density, leading to the expectation that they can effectively absorb negatively charged molecules. In this study, Eosin-Y[14] (**Figure 2-11a**) with negative charges served as the model molecule to evaluate the adsorption properties of the FPC LbL nanofilms using QCM. As shown in **Figure 2-11c**, the frequency decreased immediately after injecting the Eosin-Y into the QCM sensor, indicating the adsorption of Eosin-Y to the nanofilms. The frequency reached a plateau after 1 h. After rinsing with Milli-Q water there was a residual frequency decrease of 339 Hz, corresponding to the mass deposition of 210 ng/cm^2. In contrast, the control group that was injected with the same volume of Milli-Q water showed no frequency decrease. The same experiment was also conducted on polyelectrolyte (PE) LbL nanofilms fabricated with PLL and PAA. As shown in **Figure 2-11d**, even with the positive-charged out layer, there is almost no Eosin-Y was absorbed to the PE LbL nanofilms. The higher adsorption property of the FPC LbL nanofilms is attributed to their charge density and

distribution. As shown in **Figure 2-11b**, FPC LbL nanofilms preserved the positive charges during the film assembly, so the charges were distributed both inside and on the surface of the films. However, the PE LbL nanofilms consumed the charges along the polymer to form electrostatic interactions with their opposites, resulting in a neutral environment inside the films. The unique charge density and distribution of FPC LbL nanofilms provide them with higher adsorption properties.

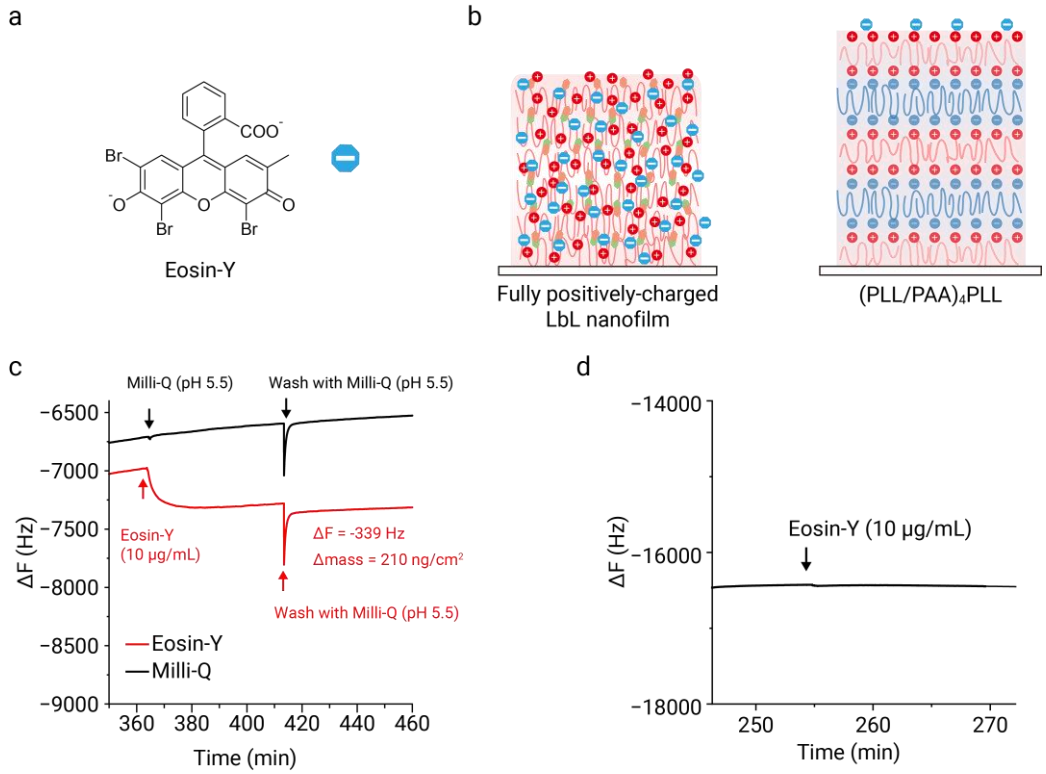

Figure 2-11 Adsorption properties of FPC LbL nanofilms. (a) Molecular structure of Eosin-Y. (b) Schematic illustration showing the advantage of FPC LbL nanofilms in absorbing negatively-charged molecules compared with polyelectrolyte LbL nanofilms. (c) Frequency shift of (PLL-EG$_4$-Azi/PLL-EG$_2$-Alk)$_5$ LbL nanofilms after adding Eosin-Y solution (10 μg/mL), and then washing by Milli-Q water (pH 5.5). The concentrations of polymers were 0.16 mg/mL. (d) Frequency shift of (PLL/PAA)$_4$PLL LbL nanofilms after adding Eosin-Y (10 μg/mL). The concentrations of polymers were 0.16 mg/mL.

After the QCM measurement, the fluorescence intensity of QCM sensors was measured to further demonstrate the adsorption of Eosin-Y. **Figure 2-12a** shows the effective measurement part of the QCM sensor, where both polymer deposition and molecule adsorption on the golden center part were measured. After absorbing Eosin-Y, a stronger

fluorescence was observed (**Figure 2-12c**). The fluorescence intensities of the images were measured across the white guideline in **Figure 2-12c**. The QCM sensor that absorbed Eosin-Y showed a fluorescence signal all over the sensors, but there was no fluorescence signal over the control QCM sensor that adding Milli-Q water (**Figure 2-12b**), suggesting the successful adsorption of negatively-charged molecules.

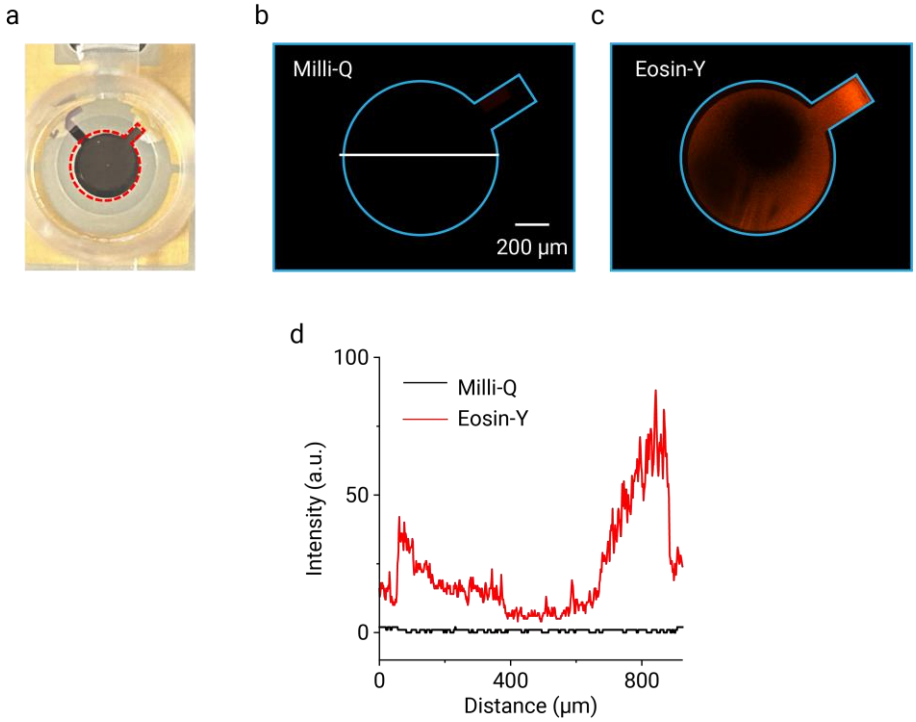

Figure 2-12 (a) A digital photo of the QCM sensor, the region in the red dashed line is where the polymers were deposited. (b-c) Fluorescence images of QCM sensors after the adsorption experiments. (b) Milli-Q water, (c) Eosin-Y. The images were taken with the same excitation strength and masked to only show the effective measurement region. (d) Linear scanning of the intensity profile along the white line of the QCM sensors after the adsorption experiments.

2.4 Conclusion

In conclusion, fully-positively charged (FPC) LbL nanofilms were prepared via CuAAC click reaction. The high specificity and efficient reaction overcame the electrostatic repulsions within PLL. Compared with conventional PE LbL nanofilms, the FPC LbL nanofilms contained free ionic amino groups all over the nanofilms, which could respond to pH changes. The different state of amino groups resulted in the thickness and surface morphology switch of the nanofilms. In addition, the stable covalent bond between individual layers improved the robustness of the nanofilms. The unique high positive charge density promoted the adsorption

of negatively-charged molecules. This work takes advantage of the controllability of the LbL assembly method and the high efficiency of CuAAC click reaction, suggesting the possibility that these methods could be used to design and fabricate functional LbL nanofilms, with potential application in charge-related fields like molecule adsorption, permeation, and drug delivery.

Our group has successfully fabricated both fully negatively-charged (FNC) LbL nanofilms[1] and FPC nanofilms. These nanofilms exhibit higher charge density, enhanced pH stability and greater pH responsiveness compared to the traditional polyelectrolyte (PE) nanofilms. The opposite charges of FNC and FPC nanofilms allow for the different applications. Additionally, due to the limitation of the instability of Cu ions, the FPC nanofilms were fabricated in pH 5.5, where PLL were not fully deprotonated. So, the FPC nanofilms are thinner than FNC nanofilms. Currently, we use the weak amine and weak acid for the fully single-charged nanofilm fabrication. If we were about to the strong acid, such as poly(styrene sulfonate) (PSS), and strong ammonium, , such as poly(diallyldimethylammonium chloride) (PDDA), it could be possible to fabricate pH-independent nanofilms. These nanofilms would maintain a consistently high charge density regardless of pH variations. This strategy can also be extended to other click reactions, such as copper-free click reaction. Such extension can overcome the limitations of Cu ions and expand the application of single charged LbL nanofilms in biomedical fields.

2.5 References

[1] Z. Zhang, J. Zeng, W. Li, M. Matsusaki, *Chem. Mater.* **2024**, *36*, 1947.

[2] N. Cheng, Y. Zhang, Y. Wu, B. Li, H. Wang, S. Chen, P. Zhao, J. Cui, X. Shen, X. Zhu, Y. Zheng, *Mater. Today Bio* **2022**, *17*, 100476.

[3] M. Malkoch, R. Vestberg, N. Gupta, L. Mespouille, P. Dubois, A. F. Mason, J. L. Hedrick, Q. Liao, C. W. Frank, K. Kingsbury, C. J. Hawker, *Chem. Commun.* **2006**, 2774.

[4] K. Kadowaki, M. Matsusaki, M. Akashi, *Langmuir* **2010**, *26*, 5670.

[5] J. Zeng, N. Sasaki, C. R. Correia, J. F. Mano, M. Matsusaki, *Small* **2020**, *16*, 1907434.

[6] L. Jierry, N. Ben Ameur, J.-S. Thomann, B. Frisch, E. Gonthier, J.-C. Voegel, B. Senger, G. Decher, O. Felix, P. Schaaf, P. Mesini, F. Boulmedais, *Macromolecules* **2010**, *43*, 3994.

[7] A. Nebbioso, P. Mazzei, *Magn. Reson. Chem.* **2016**, *54*, 937.

[8] X. Wang, R. Wang, F. Wu, H. Yue, Z. Cui, X. Zhou, Y. Lu, *Eur. Polym. J.* **2021**, *158*, 110689.

[9] J. J. Richardson, M. Björnmalm, F. Caruso, *Science* **2015**, *348*, aaa2491.

[10] Y. Zhan, W. Fu, Y. Xing, X. Ma, C. Chen, *Mater. Sci. Eng. C* **2021**, *127*, 112208.

[11] Z. Shao, Q. Liu, *Extreme Mech. Lett.* **2023**, *64*, 102085.

[12] D. A. Roberts, B. S. Pilgrim, T. N. Dell, M. M. Stevens, *Chem. Sci.* **2020**, *11*, 3713.

[13] M. Zheng, M. Pan, W. Zhang, H. Lin, S. Wu, C. Lu, S. Tang, D. Liu, J. Cai, *Bioact. Mater.* **2021**, *6*, 1878.

[14] V. R. Batistela, D. S. Pellosi, F. D. de Souza, W. F. da Costa, S. M. de Oliveira Santin, V. R. de Souza, W. Caetano, H. P. M. de Oliveira, I. S. Scarminio, N. Hioka, *Spectrochim. Acta. A. Mol. Biomol. Spectrosc.* **2011**, *79*, 889.

Chapter 3 In-situ LbL assembly of fully negatively-charged nanofilms on living cell surface

3.1 Introduction

Chapter 1 introduced the fabrication of fully single-charged LbL nanofilms using negatively-charged poly (acrylic acid) (PAA) as the backbone and CuAAC as the driving force to overcome electrostatic repulsion. Compared to polyelectrolyte (PE) LbL nanofilms, the fully negatively-charged (FNC) nanofilms showed extraordinary pH-responsive properties and high capacity of loading positively-charged molecules due to the high negative charge density.[1]

However, the requirement of cytotoxic copper ions[2,3] limits the application of in-situ LbL assembly of FNC nanofilms on the cell surface. In-situ LbL on a cell surface has wide applications like cell compartmentalization[4] and increasing the cell viability.[5] Strain-promoted alkyne-azide cycloaddition (SPAAC) of azide and cyclooctyne as a copper-free and biorthogonal click reaction can occur in living cells without interfering with normal cellular processes.[6] Due to the high selectivity and no additional reagents, this reaction is a useful tool to realize in-situ LbL assembly on a cell surface. In this study, we chose negatively-charged PAA as the polymer backbone, and exploited the reactivity between azide and dibenzocyclooctyne (DBCO) under physiological conditions to deposit Cu-free FNC LbL nanofilms on living cell surfaces (**Figure 3-1**). We suggest that covalent binding of azide and DBCO can overcome the electrostatic repulsion between deprotonated carboxyl groups of PAA. Compared to the traditional PE films, the FNC nanofilms with high charge density have been proved to show higher loading capacity to positive-charged molecules,[1] that can be used for the drug and growth factor loading in tissue engineering. The FNC nanofilms avoid the use of polycations, which are cytotoxic by disrupting cell membrane.[7] Even the outmost layer negative-charged, the leakage polycations from the PE nanofilms in the physiological environment remains a risk. The fabrication and further application of FNC LbL nanofilms avoid the cytotoxicity of polycations. To the best of our knowledge, this is the first research to report fabrication of FNC LbL nanofilms on living cell surfaces.

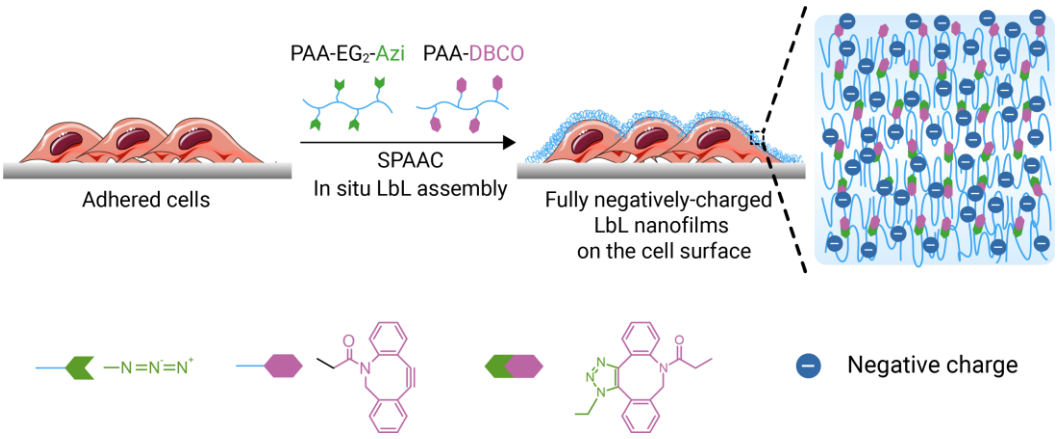

Figure 3-1 Schematic illustration of in situ LbL assembly of Cu-free FNC LbL nanofilms on cell surface based on SPAAC reaction.

3.2 Experiment

3.2.1 Materials

Poly (acrylic acid) (PAA, 25 kDa) hydrochloric acid (HCl, 5M), sulfuric acid (H_2SO_4, 95.0%), and Paraformaldehyde (PFA) were purchased from Wako Pure Chemical Industries. 2-[2-(2-Azidoethoxy)ethoxy] ethanamine (azide-EG_2-amine, 95%), and Cy5-amine were purchased from BroadPharm. Dibenzocyclooctyne-amine (DBCO-amine, >95%) was purchased from TCI. 4-(4,6-Dimethoxy-1,3,5-triazin-2-yl)-4-methyl morpholinium chloride (DMTMM, 97.5%) was purchased from Watanabe. Fluorescein glycine amide (FGA) was purchased from Funakoshi. Phalloidin-iFlor 555 was purchased from Abcam. Hoechst33342 was purchased from Thermo Fisher Scientific. 1x PBS 7.4 (PBS 7.4) was prepared by dissolving PBS powder (D-PBS without Ca and Mg, Powder from Nacalai tesque, INC.) to Milli-Q water.

3.2.2 Synthesis of PAA-EG_2-Azi

PAA functionalized with various contents of azide groups as synthesized via DMTMM-mediated coupling of carboxyl groups of PAA with azide-EG_2-amine. 60 mg (0.83 mmol) of PAA as dissolved in 12 mL of sodium borate buffer (pH 8.5, 0.5 M). 460.8 mg (1.66 mmol) of DMTMM was added to the solution together with 36.3 mg (0.21 mmol) of azide-EG_2-amine to produce PAA-EG_2-Azi with 25 % azide feeding ratio. The solution was stirred at room temperature for 24 hours, then dialyzed against Milli-Q water and freeze-dried to get the final product.

3.2.3 Synthesis of PAA-DBCO

DBCO was conjugated to PAA via DMTMM-mediated coupling reaction. PAA (50 mg, 0.69 mmol) was mixed with DMTMM (192 mg. 0.69 mmol) in 13.33 ml of carbonate buffer solution (pH 8.5, 0,1 M) for 10 min. DBCO-amine (19.2 mg, 0.069 mmol) dissolved in 3.33 mL of THF. Then add to the mixture solution dropwise. The reaction kept stirring at room temperature for 24 hours. The product was purified via dialysis (MWCO: 8000) against Milli-Q water, methanol, and Milli-Q water for 1 day each.

3.2.4 Click reaction monitoring using UV-vis absorbance.

PAA-EG_2-Azi and PAA-DBCO were dissolved in 1X PBS to obtain the polymer solution with the concentration of 3.2 mg/mL and 0.32 mg/mL respectively. 1.5 mL of PAA-EG_2-Azi and PAA-DBCO solutions were mixed in a cuvette, then pipetting 5 times. After mixture, the concentration of PAA-EG2-Azi and PAA-DBCO changed to 1.6 mg/mL and 0.16 mg/mL. the UV-Vis spectra were measured at a certain time interval.

3.2.5 Preparation and characteristics of Cu-free fully negative-charged layer-by-layer (LbL) nanofilm

The quantitative measurement of the LbL assembly was analyzed using a quartz crystal microbalance (QCM, AFFINIX Q8, ULVAC) as our previously reported protocol.[1] Briefly, QCM sensors (QCM01S, ULVAC) were treated with piranha solution (H_2SO_4:35% H_2O_2 = 3:1) for 10 min and repeated 3 times. 100 μL of PBS 7.4 was added to the cells until the frequency was stable. 5 μL of the concentrated PAA-EG_2-Azi **(**3.36 mg/mL, PBS 7.4**)** solutions was added to the cells and diluted to the desired concentration (0.16 mg/mL). After 15 min of deposition, PAA-EG_2-Azi solutions were removed, and the sensors were rinsed with PBS 3 times. Then the frequency was stabilized in new PBS, 5 μL of the concentrated PAA-DBCO **(**3.36 mg/mL, PBS 7.4**)** solutions was added into the cell s for the second layer assembly. By alternating switch the polymer solutions, nanofilms were assembled on the QCM sensors. The frequency shift (ΔF) was recorded, and the deposited mass (Δm) was calculated based on the Sauerbrey equation[8]:

$$-\Delta m(ng\ /\ cm^2) = 0.62\Delta F(\mathrm{Hz}) \qquad (3-1)$$

The pH-responsive measurement and stability evaluation of LbL nanofilms were accessed in situ by QCM. After film fabrication, they were incubated in 100 μL PBS 7.4 or PBS 6.5.

3.2.6 AFM observation

For the AFM (Shimadzu, SPM-Nanoa) measurement, layer-by-layer nanofilms were fabricated on silicon wafers (As one, 2-960-05). (AFM measurement mode: Dynamic (lq); probe: OMCL-AC200TS-C3)

3.2.7 Cell culture

NHDF (passage 9-11) were cultured with DMEM containing 10% FBS and 1% penicillin/streptomycin in 5 % CO_2 at 37 °C.

3.2.8 Cell viability

The viability of NHDF with Cu-free nanofilms was performed using a Live/Dead viability assay kit and WST-8 kit assay. For Live/Dead viability assay kit, 1.0×10^5 NHDF were seeded in each well (24-well plate) and then incubated at 37 °C for 24 h. LbL nanofilms were assembled on the cell surface and incubated for another 24 h. After further washing with PBS, 300 μL of PBS solution containing Calcein AM (1 μM) and EthD-1 (2 μM) was added into each well, followed by incubation at 37 °C for 45 min in the dark. After incubation, each well was rinsed with PBS 3 times. Images were obtained using a confocal laser scanning microscope.

For WST-8 kit assay, 100 μL of 1.0×10^4 NHDF were cultured in 96-well plate at 37 °C for 24 h. Then nanofilms were assembled on the cell surface and incubated for another 24 h. After incubation, the cells were washed with PBS 3 times, 100 μL of cell count reagent SF/DMEM (1:9) was added to each well. The cells were incubated for another 3 h at 37 °C. And then transferring the supernatant to a new well, the absorbance of supernatant at 450 was measured by microplate reader. The cell numbers after LbL were counted by trypan blue staining. The normalized cell viability was calculated.

3.2.9 In-situ layer-by-layer on cell surface

LbL nanofilms were assembled on the top of fibroblasts. To distinguish the cells and nanofilms. 2 mL of 2×10^6 NHDF was incubated in a 35 mm glass-bottom dish for 24 h. After washing with PBS 3 times, 2 mL FGA-PAA-EG_2-Azi and Cy5-PAA-DBCO with the concentration of 0.16 mg/mL were deposited alternately on the NHDF surface for 5 bilayers and incubated in 2 mL DMEM (10% FBS, 1% anti) at 37 °C for 24 h. Cells and nanofilms were observed with confocal laser scanning microscope (FluoView FV3000). The results

were analyzed by Imaris and ImageJ.

3.2.10 Actin Staining

After LbL on the NHDF surface and incubated for 24 h, samples were washed with PBS 3 times and fixed by 4% paraformaldehyde (PFA) for 15 min at room temperature. After washing with PBS 3 times, the samples were incubated with Phalloidin-iFlor 555 in 1% BSA/PBS solution at room temperature for 2 h. The nuclei were counterstained with Hoechst33342. After washing with PBS 3 times, the samples were observed with a confocal laser scanning microscope.

3.2.11 Safranin O (SO) adsorption

NHDF coated with $(PAA\text{-}EG_2\text{-}Azi/PAA\text{-}DBCO)_5$ (10 layers), $PAA\text{-}EG_2\text{-}Azi$ (1 layer), and without nanofilms (Control) were cultured. Samples were incubated in 10 μg/mL of Safranin O (SO)/PBS for 30 min in the dark. After incubation, the fluorescent intensities of supernatants were measured. The cell samples were washed with PBS 3 times then observed by FV3000. The linear scanning of the fluorescence intensity was measured using ImageJ.

3.2.12 Characterization methods and statistic

The chemical structure of the functionalized polymers was analyzed by ^{1}H-NMR (Jeol, JNM-GSX 400, Japan). Fluorescence images were observed with confocal laser scanning microscopy (CLSM, FV300, Olympus, Japan). The AFM observing cells were conducted using 3D mapping in PBS 7.4 (Probe: CONT, Nanoworld).

3.2.13 Statistical analysis

All values are presented as means ± standard deviation (SD). Statistical analysis of the data was performed with Student's *t*-test or One-way *ANOVA.*

3.3 Results and discussions

3.3.1 Synthesis of PAA-EG2-Azi

The synthesis of $PAA\text{-}EG_2\text{-}Azi$ was same as introduced in section 1.2.2.

3.3.2 Synthesis of PAA-DBCO

DBCO-amine was conjugated to polyacrylic acid (PAA), a negatively-charged polyelectrolyte. Briefly, the carboxyl groups of PAA were activated using (4,6-Dimethoxy-

1,3,5-triazin-2-yl)-4-methyl morpholinium chloride (DMTMM) as a coupling agent, then conjugated to DBCO amine (**Figure 3-2a**). ^{1}H-NMR spectra confirmed the successful synthesis of PAA-DBCO with a 9% graft ratio (**Figure 3-2b**).

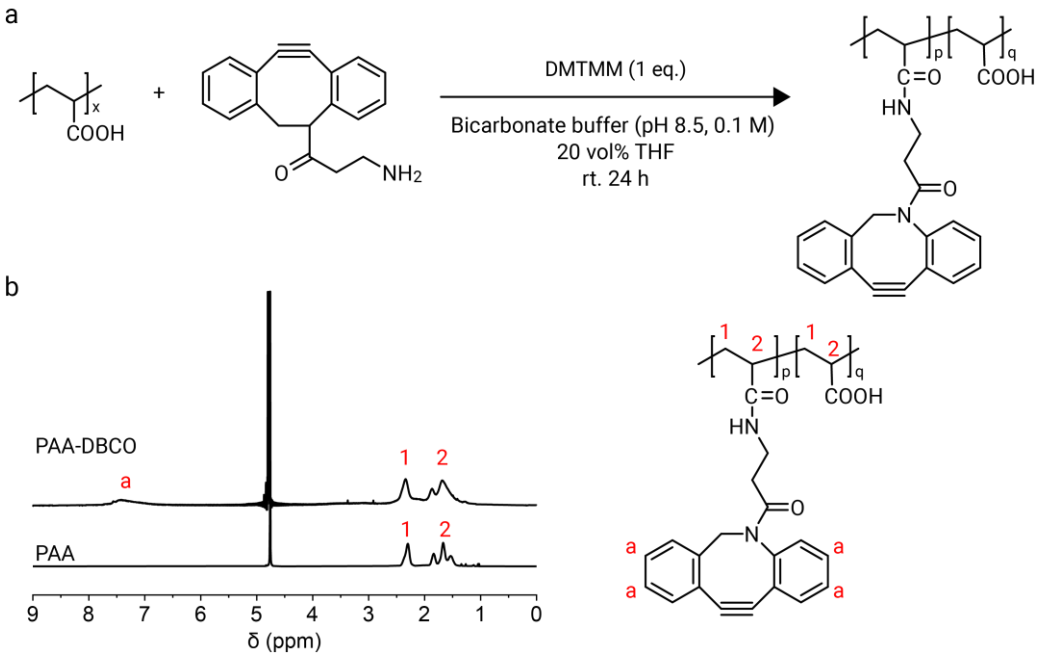

Figure 3-2 (a) Synthesis of PAA-DBCO. (b) ^{1}H-NMR (400 MHz, D_2O, 25 °C) spectra of PAA-DBCO, and PAA

3.3.3 Real-time SPAAC click reaction Monitoring

The SPAAC reaction between the two polymers was confirmed by UV-vis spectrophotometry. PAA-EG_2-Azi (final concentration: 1.6 mg/mL) and PAA-DBCO (final concentration: 0.16 mg/mL) were mixed in a PBS 7.4 and the reaction was monitored by observing the change in the UV-vis spectrum of the mixture (**Figure 3-3a**). The UV-vis absorbance was measured every 10 min for the first 2 h, then every 30 min thereafter. As the reaction proceeded, due to the structural change of a cyclooctyne into a triazole (**Figure 3-3a**), the characteristic absorbance peak of DBCO at 310 nm gradually decreased (**Figure 3-3b**).

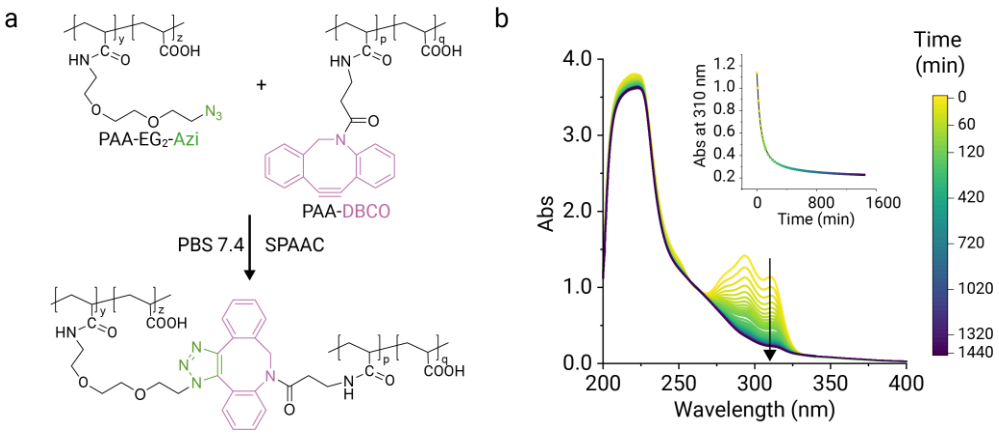

Figure 3-3 SPAAC reaction between PAA-EG$_2$-Azi and PAA-DBCO. (c) Absorbance spectra throughout the SPAAC reaction. Inserted: absorbance time series at 310 nm. The reaction was run with 0.16 mg/mL PAA-DBCO and 1.6 mg/mL PAA-EG$_2$-Azi in PBS 7.4.

3.3.4 Characteristics of Cu-free fully negatively-charged LbL nanofilms

The fabrication of FNC LbL nanofilms was based on the efficient and irreversible SPAAC between PAA-EG$_2$-Azi and PAA-DBCO. By alternately exposing the substrate to different functionalized polymer solutions, the SPAAC reaction led to the absorption of polymer to the pre-layer (**Figure 3-4a**). LbL assembly of the nanofilms was monitored by quartz crystal microbalance (QCM). As expected, the frequency shift (ΔF) increased with the alternate exposure of the QCM sensor to PAA-EG$_2$-Azi and PAA-DBCO (**Figure 3-4**b), confirming the layer-by-layer deposition of polymers. The 5-bilayer nanofilm showed a total ΔF of 1074 Hz. Unlike PE LbL nanofilms that dissociate when the pH breaks the electrostatic interactions between layers,[1] the Cu-free FNC nanofilms were able to maintain the interactions even in a harsh pH environment due to the covalent bonding between the azide and DBCO (**Figure 3-4c**), showing good stability.

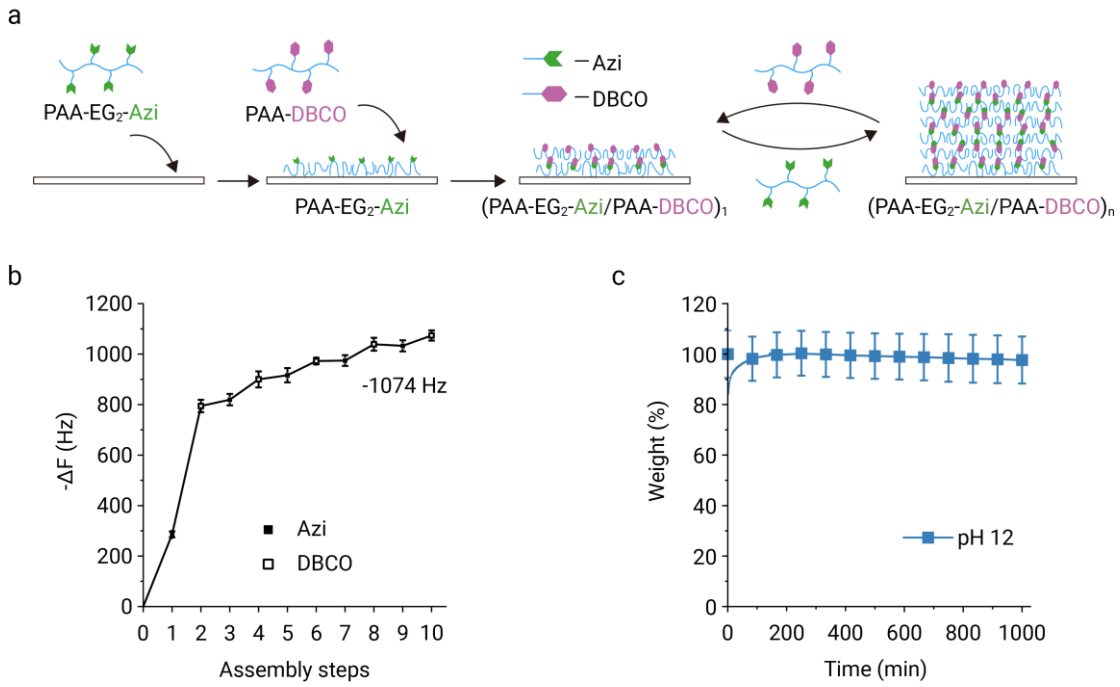

Figure 3-4 Characteristics of Cu-free FNC LbL nanofilms (a) Schematic illustration of Cu-free FNC LbL nanofilm fabrication (b) Frequency shifts (ΔF) of (PAA-EG$_2$-Azi/PAA-DBCO)$_5$ LbL nanofilm at each step (n=3). (c) Stability of (PAA-EG$_2$-Azi/PAA-DBCO)$_5$ LbL nanofilm incubating in pH 12 solutions.

The Cu free FNC LbL nanofilms contained a large number of free carboxyl groups, which are sensitive to pH changes. When we changed the pH of the PBS on the QCM sensors, the ΔF showed a cyclic fluctuation between the average value of 964 and 494 Hz (**Figure 3-5a**), indicating the swelling of FNC nanofilms at pH 7.4 and shrinking at pH 6.5. The thickness and surface roughness of the 5-bilayer nanofilm was evaluated by AFM at different pH (**Figure 3-5c and e)**. The height profile revealed the thickness of the nanofilm was 22.8 nm in PBS 7.4 (**Figure 3-5d**) and 16.3 nm in PBS 6.5 (**Figure 3-5e**). The results showed the same trend as the QCM measurement. Additionally, nanofilms in PBS 7.4 (Ra: 0.24 nm) showed a lower surface roughness than in PBS 6.5 (1.38 nm). With the pKa of PAA around 4.5,[9] the pH sensitivity was related to the ratio of protonated and deprotonated free carboxyl groups in the nanofilms. As shown in **Figure 3-5b**, higher pH increased the ratio of deprotonated carboxyl groups, increasing both intermolecular and intramolecular electrostatic repulsion, leading to a swelling of the nanofilms. Conversely, lower pH resulted in less repulsion, and increased the hydrogen bond between some protonated carboxyl groups, allowing the nanofilms to shrink and form a more collapsed polymer conformation[10,11] on the

surface of the agglomerates.

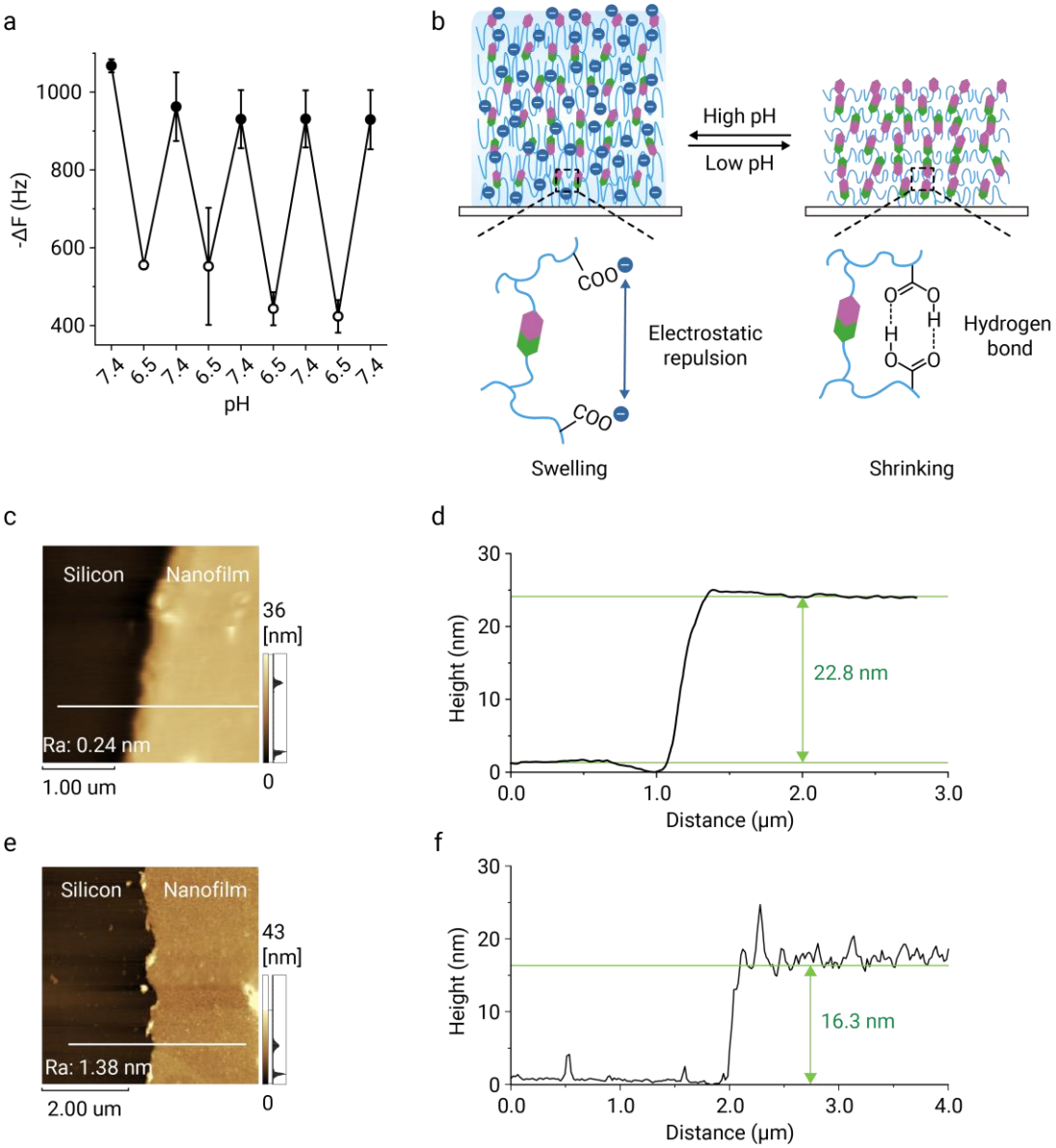

Figure 3-5 (a) Negative frequency shifts (-ΔF) of $(PAA\text{-}EG_2\text{-}Azi/PAA\text{-}DBCO)_5$ LbL nanofilm in PBS 7.4 and PBS 6.5. (b) Schematic depicting the pH responsive properties. (c-f) AFM height image of $(PAA\text{-}EG_2\text{-}Azi/PAA\text{-}DBCO)_5$ LbL nanofilm in PBS 7.4 (c) and PBS 6.5 (e). The corresponding height profile across the scratched edge and surface roughness (Ra) of LbL nanofilm in PBS 7.4 (d) and PBS 6.5 (f). The concentration of the polymer is 0.16 mg/mL.

3.3.5 In-situ fabrication of Cu-free FNC LbL nanofilms on living cell surface

Normal human dermal fibroblasts (NHDF) were seeded on glass-bottomed dishes then

cultured for 24 h to make the cells attach to the substrates. (PAA-EG_2-Azi/PAA-DBCO)$_5$ nanofilms were assembled on the attached cells following the same protocol as on the QCM sensors (**Figure 3-6a**). After 24 h of nanofilm deposition on the cell surface, initial viability tests were then performed via live/dead staining and WST-8 assay. Cells coated with nanofilms showed no decrease in viability compared with the control group, suggesting cytocompatibility of the nanofilms (**Figure 3-6b** and **c**).

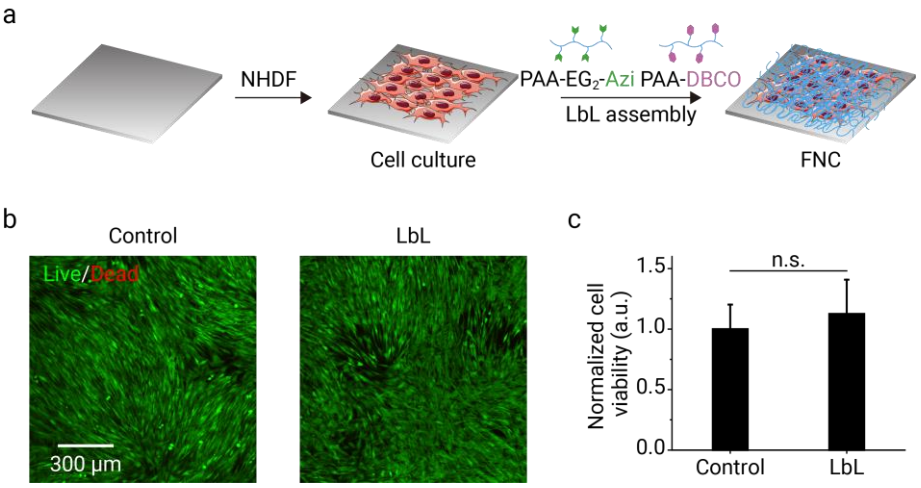

Figure 3-6 Cu-free FNC LbL nanofilms in situ assembled on cell surface. (a) Schematic image of LbL assembly process of (PAA-EG_2-Azi/PAA-DBCO)$_5$ nanofilms on cell surface. (b) CLSM images of living cells stained by Calcein AM (green) and dead cells stained by ethidium homodimer-1 (red). (c) Normalized cell viability after 24 h incubating without (Control) and with (LbL) nanofilms assembled on the cell surface. Data are presented as means ± S.D. Statistical analysis was performed using Student t-test. (n.s. $p \geq 0.05$)

The localization of the nanofilms on the living cell surface was investigated. As shown in **Figure 3-7**, the polymers formed a continuous network consisting of fibers. Fluorescence signals of FGA-PAA-EG_2-Azi completely overlapped with Cy5-PAA-DBCO. This observation suggested that two different functionalized PAA were localized at the same place, indicating the highly specific interaction between azide and DBCO. Nanofilm signals partially overlapped with cells after 24 h of incubation, meaning that the nanofilms interacted with the cell surface. The co-incubation for 24 h also suggests the stability of LbL nanofilms in cell culture medium. From the high magnification images, as shown in **Figure 3-7**, the NHDF cells showed normal cell morphology, suggesting the presence of nanofilms on the cell surface didn't affect the cell behavior.

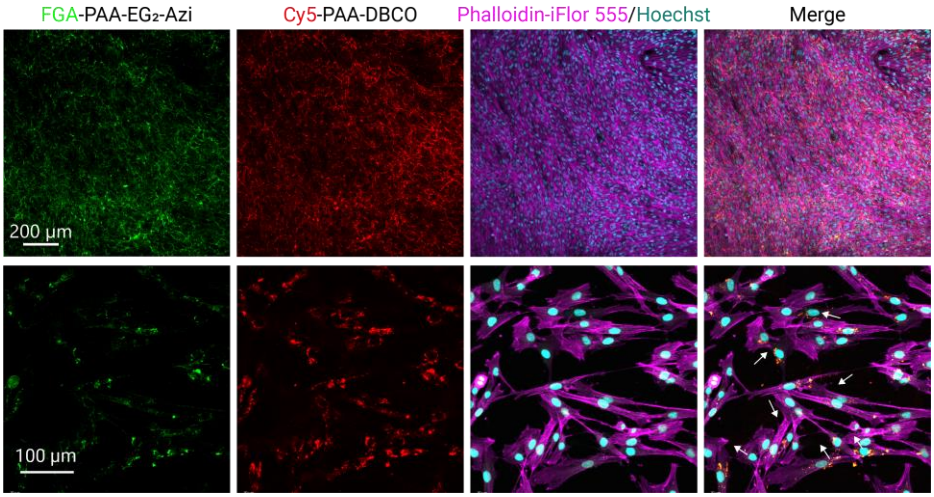

Figure 3-7 CLSM images with different magnification of the (FGA-PAA-EG_2-Azi/Cy5-PAA-DBCO)$_5$ LbL nanofilms deposited on the cell surface and then incubated for 24 h. (Green: FGA, red: Cy5, violet: Phalloidin-iFlor 555, cyan: Hoechst). White arrows indicated the overlapping of nanofilms and cells. The concentration of the polymer is 0.16 mg/mL.

Upon successfully confirming the in situ assembly of nanofilms on the cell surface, we next investigated whether this nanofilm coating could affect the properties of the cell surface. Therefore, AFM was used to quantify membrane adhesion of NHDF in PBS. As shown in **Figure 3-8**, from the height images, fibers-shaped nanofilms over the cell surface and in between the gap of neighboring cells were observed after LbL assembly, matching the results shown in the CLSM images (**Figure 3-7**), further indicating the successful assembly of nanofilms. The maps of adhesion force exhibited heterogeneous distribution of adhesion behavior where the region around the cell's center possessed a higher adhesion force. In addition, compared with the control group, the adhesive force of the LbL group was markedly lower. The tips of the AFM probes are slightly negatively charged,[12] so after the fabrication of our FNC nanofilms on the cell surface, the cell coated with nanofilms attracted the tip less than cells without nanofilms, resulting in a decrease of adhesive force. This confirms the nanofilm can change the surface charges of cells to a more negative state. The ability to absorb positively-charged molecules might be applied to load biofactors or drugs that are used to further regulate the cell behavior. Besides, the FNC nanofilms on the surface might serve as a shell to prevent the cell being harmed by positively-charged polymers.

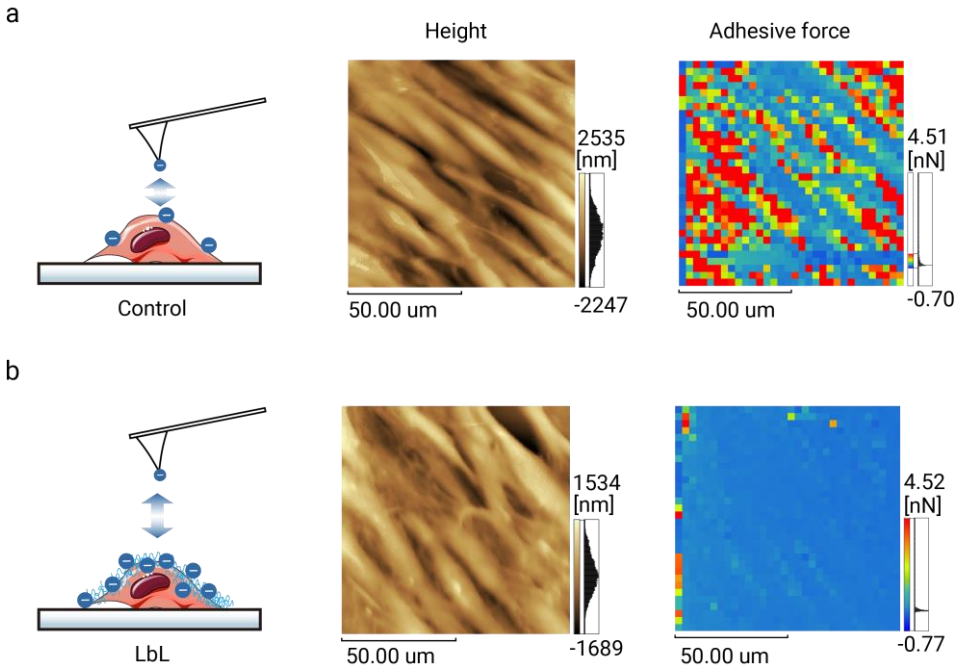

Figure 3-8 AFM height images and adhesive force map of the same cell surface area without nanofilms (a) and with nanofilms (b). Cells were fixed with 4% PFA and were measured in PBS 7.4.

3.3.6 Adsorption properties of cells coated with FNC LbL nanofilms

The abundant negative charges on the cell surface led to the expectation that nanofilms could effectively absorb positively-charged molecules (**Figure 3-9b**). Here, we used positive-charged Safranin O (SO) (**Figure 3-9a**) as the model drug or growth factor, with a distinct emission wavelength from that of fluorescent labelled polymers to evaluate the adsorption properties of the FNC nanofilms on the cell surface. For a better comparison, we also prepared samples with only 1 layer of PAA-EG_2-Azi deposited on the cell surface. The as prepared samples were incubated in SO solutions for 30 min then the excess SO was washed away using PBS. For the control groups without nanofilms, SO can only be absorbed by the negative charges on the cell surface, [13] thus fluorescence signals only show on top in the area where the cell attached (**Figure 3-9c**, upper line). For the cells coated with only one PAA-EG_2-Azi layer (**Figure 3-9**, middle line), the partial overlap of polymer and SO signals can be observed, indicate the adsorption of SO of the polymer layer. The cells coated with 10 layers (PAA-EG_2-Azi/PAA-DBCO)$_5$ effectively absorbed SO via electrostatic interaction on the surface (**Figure 3-9**c, lower line) and the location where nanofilms deposited exhibited an especially high fluorescence intensity of SO.

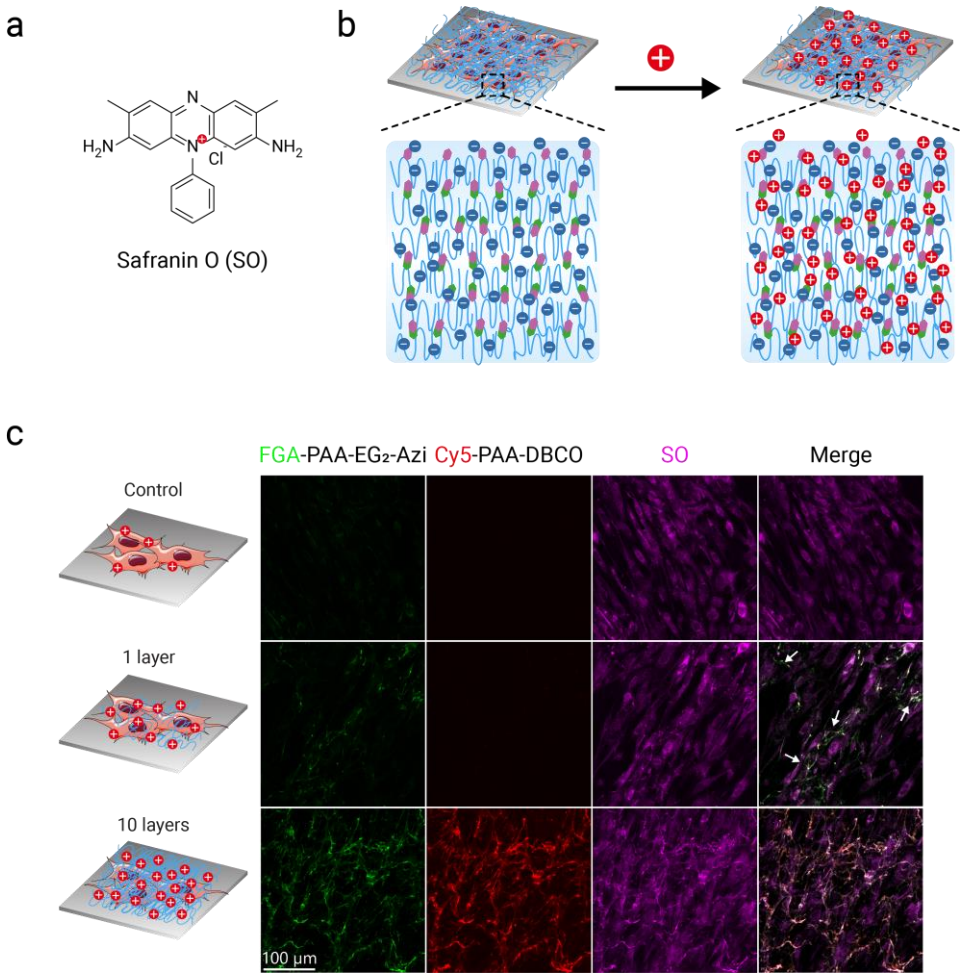

Figure 3-9 Adsorption properties of Cu-free FNC LbL nanofilms on cell surface. (a) Molecular structure of Sarafin O (SO). (b) Scheme illustration showing the adsorption of SO by FNC nanofilms. (c) CMSL images of cells without nanofilms (control, upper line), with PAA-EG_2-Azi (1 layer, middle line) and (PAA-EG_2-Azi/PAA-DBCO)$_5$ (10 layers, lower line) obtained after 30 min incubation in the solutions of SO (10 μg/mL). (Green: FGA, red: Cy5, violet: SO).

The location of polymers and SO were investigated by analyzing the fluorescent image (**Figure 3-10a**) using ImageJ. The result is shown in **Figure 3-10b**, the overlapped peak of the fluorescence profile of polymers and SO demonstrated the location. Quantitative assessment of the adsorption performance of the samples during incubation of SO solutions demonstrated that the FNC nanofilms deposited on the cell surface increased the SO uptake to about 1.76 times that of the control groups.

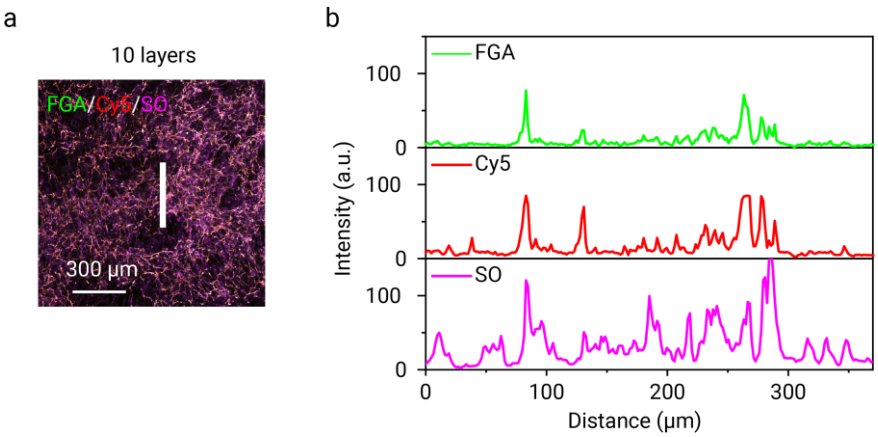

Figure 3-10 (a) Merged CMSL image of cells coated with (PAA-EG$_2$-Azi/PAA-DBCO)$_5$ nanofilms after 30 min incubation in SO. (Green: FGA, red: Cy5, violet: SO). (b) Linear scanning of the fluorescence intensity profiles along the white line of the image.

3.4 Conclusion

In conclusion, we fabricated a Cu-free FNC LbL nanofilm based on SPAAC click reaction and achieved in-situ assembly on a living cell surface. We confirmed the reaction between PAA-EG$_2$-Azi and PAA-DBCO in PBS 7.4. LbL assembly was successfully realized both on the inorganic substrate and on a living cell surface. The FNC nanofilms showed pH responsiveness on the thickness and surface morphology. Fluorescence-labeled polymer and cell staining confirmed the successful deposition of nanofilms on the cell surfaces. AFM force mapping showed that the nanofilms markedly reduced the cell surface adhesion without affecting the cell viability and morphology. The surface modification on the cell with FNC nanofilms with abundant negative charges allows them to possess a higher capacity of positively-charged molecules for further applications. This is the first report of FNC LbL nanofilms on a cell surface.

3.5 References

[1] Z. Zhang, J. Zeng, W. Li, M. Matsusaki, *Chem. Mater.* **2024**, *36*, 1947.

[2] M. C. Cortizo, M. F. L. De Mele, *Biol. Trace Elem. Res.* **2004**, *102*, 129.

[3] E. Mavil-Guerrero, R. Vazquez-Duhalt, K. Juarez-Moreno, *Chemosphere* **2024**, *347*, 140713.

[4] J. Zeng, N. Sasaki, C. R. Correia, J. F. Mano, M. Matsusaki, *Small* **2020**, *16*, 1907434.

[5] D. Choi, H. Lee, H.-B. Kim, M. Yang, J. Heo, Y. Won, S. S. Jang, J. K. Park, Y. Son, T. I. Oh, E. Lee, J. Hong, *Chem. Mater.* **2017**, *29*, 2055.

[6] J. C. Jewett, E. M. Sletten, C. R. Bertozzi, *J. Am. Chem. Soc.* **2010**, *132*, 3688.

[7] M. Wytrwal-Sarna, P. Knobloch, S. Lasota, M. Michalik, M. Nowakowska, M. Kepczynski, *Environ. Sci. Nano* **2022**, *9*, 702.

[8] G. Sauerbrey, *Z. Für Phys.* **1959**, *155*, 206.

[9] D. Yoo, S. S. Shiratori, M. F. Rubner, *Macromolecules* **1998**, *31*, 4309.

[10] M. Todica, R. Stefan, C. V. Pop, L. Olar, *Acta Phys. Pol. A* **2015**, *128*, 128.

[11] D. G. Mintis, V. G. Mavrantzas, *J. Phys. Chem. B* **2019**, *123*, 4204.

[12] L. Li, N. F. Steinmetz, S. J. Eppell, F. R. Zypman, *Langmuir* **2020**, *36*, 13621.

[13] M. Nishino, I. Matsuzaki, F. Y. Musangile, Y. Takahashi, Y. Iwahashi, K. Warigaya, Y. Kinoshita, F. Kojima, S. Murata, *PLoS ONE* **2020**, *15*, e0236373.

Concluding remarks

In this thesis, a series of fully single charged layer-by-layer nanofilms were fabricated using only one type of polyelectrolytes.

In chapter 1, the author presented a novel approach by employing click moiety-functionalized poly (acrylic acid) (PAA) to achieve LbL nanofilms with preserved charges. The film assembly was driven by copper-catalyzed azide-alkyne cycloaddition (CuAAC), thereby yielding fully negative-charged (FNC) nanofilms possessing unique properties compared to conventional PE nanofilms, including high stability over a wide pH range (pH 2-12) and reversible pH-induced remarkable swelling-shrinking properties in response to cyclic transitions between alkaline and acidic conditions. The swelling induced by the increase in pH reached 201% with a thickness change from 138 (pH 2) to 278 (pH 12) nm. AFM measurements showed distinct morphological changes for nanofilms post-treated by solutions with different pH and structure colors depending on pH were observed. This kind of FNC nanofilm hold high potential for application as a diagnostic nanomaterial such as positive-charged ions and molecules in biomedical and environmental fields.

In chapter 2, the preparation of LbL nanofilms with preserved positive charges via a controllable and efficient approach was achieved. To fabricate fully-positively charged (FPC) LbL nanofilms, a polycation, poly-L-lysine (PLL), was partially grafted with azide and alkyne groups. Through copper-catalyzed azide-alkyne cycloaddition (CuAAC) and the LbL procedure, nanofilms were fabricated with all the individual layers covalently bonded, improving the pH stability of the nanofilms. Because the resulting nanofilms had high charge density with positive charges both inside and on the surface, they showed unique pH-dependent swelling properties and adsorption of negatively charged molecules compared with traditional polyelectrolyte LbL nanofilms. This kind of FPC nanofilm has great potential for use in sensors, diagnostics, and filter nanomaterials in the biomedical and environmental fields.

Table 1 Comparison between PE LbL nanofilms and fully single charged LbL nanofilms.

	PE	FNC
	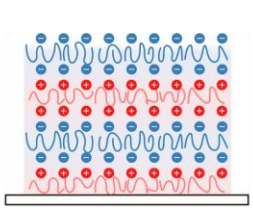	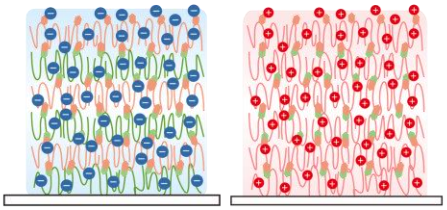
Controllable thickness	✓	✓
Thickness Growth	Exponentially	Linear
Driving force	Electrostatic interaction	Covalent bond
Stability	✗	✓
pH responsiveness	✗	✓**Thickness: repeatable and adjustable** ✓**Surface morphology**
Loading capacity	✗	✓**Improved**

In Chapter 3, considering the cytotoxicity of Cu ions and polyanions, the Cu-free FNC were fabricated and successfully deposited on living cell surfaces. The resulting nanofilms show pH responsive properties even between pH 6.5 and pH 7.4. The Cu-free FNC nanofilms coating on the cell surface didn't affect the normal cell morphology and improved the adsorption properties to the positive-charged small molecules. This pH responsiveness and high loading efficiency enable the FNC nanofilms be applicable as the loading system in the biomedical fields.

List of publications

Chapter 1

Fabrication of Fully Negatively Charged Layer-by-Layer Nanofilms with pH-Induced Remarkable Swelling–Shrinking Properties.

Zhuying Zhang, Jinfeng Zeng, Wei Li, and Michiya Matsusaki.

Chem. Mater. 2024, 36, 1947–1956.

Chapter 2

Fabrication of Fully-positively Charged Layer-by-layer Polyelectrolyte Nanofilms with pH-Dependent Swelling Properties

Zhuying Zhang, Jinfeng Zeng, and Michiya Matsusaki.

Langmuir **2024**, *revision submitted.*

Chapter 3

In-situ Fabrication of Fully Negatively charged Layer-by-layer Nanofilms on Living Cell Surface

Zhuying Zhang, Jinfeng Zeng, and Michiya Matsusaki

Chem. Comm. **2024,** *submitted*

Supplementary publication

Review: Layer-by-layer assembly methods and their biomedical applications.

Zhuying Zhang, Jinfeng Zeng, Jürgen Groll, and Michiya Matsusaki.

Biomater. Sci. **2022**, 10, 4077-4094

Acknowledgements

This study was carried out from 2021 to 2024 at Department of Applied Chemistry, Graduate School of Engineering, Osaka University. In the past three years, I have received a lot of assistance and support during my research and daily life. I would like to appreciate all the people who have helped me in some way.

Foremost, I would like to express my sincere appreciation to my supervisor, Prof. Michiya Matsusaki for the continuous support over the last three years. For his patience, enthusiasm and intelligence on research. His effective guidance helped me in every part of the research: experiment, data analysis, and writing. His calm and gentleness inspired me not being panic all the time.

I am deeply grateful to the thesis committee: Prof Toshiyuki Kida and Prof. Yutaka Ie, who generously provided knowledge and expertise. I would like to express my appreciation to Prof. Wei Li in Texas Tech University for his insightful comments and suggestions in the experiment and data discussion.

Besides my supervisor, I am deeply grateful to Dr. Jinfeng Zeng for the continuous and very patient help in my research. Thanks to Associate Prof. Masahiko Nakamoto and Assistant Prof. Kenta Homma for the comments and suggestions. Thanks to Dr. Naoko Sasaki, Dr. Zhengtian Xie, Dr. Marie Piantino, Dr. Abdul Sisak Muhammad Asri, Dr. Quentin Muller and Dr. Yucheng Shang for their comments and guidance to my experiments.

I would like to offer my special thanks to Ms. Eri Enomoto, Ms. Chika Sugiki, and Ms. Kiyomi Lee for their kind support and help in the laboratory affairs, scholarships application and daily life.

My appreciation also goes to the previous and current fellows in Matsusaki laboratory. Thanks to Guest Associate Prof. Shiro Kitano, Guest Associate Prof. Shinji Irie, Guest Associate Prof. Akiko Takasuga,

Thanks to visiting researcher Asuka Kato, Yasuyuki Naito, Yuka Yoshinouchi, Mizuho Suzuki, and Koichi Hattori. Kazumasa Nodake, Yoshihiro Kodama, Miki Mizukami, Ryoko Oodera, Hisami Ueno. Thanks to Ms. Yukiko Sorayama, Ms. Saori Nanbu, Ms. Yuri Ide, Ms. Hideyo Okano, Ms. Chikako Yamada, Ms. Mami Kikkawa, Mr. Koji Nakade, Mr. Takuya

Sugiura, Mr. Tomoya Matsuo, Ms. Misa Miyamoto, Mr. Tamaki Kumauchi, Mr. Ryosuke Isobe, Mr. Yusuke Kajiura, Ms. Kaori Hayazaki, Mr. Kazuki Odake, Ms. Asli Sena Karanfil, Mr. Daisuke Tomioka, Mr. Yuki Koba, Ms. Chika Nakadozono, Mr. Kazuki Moroishi, Mr. Kazuki Yoshida, Ms. Sukulya Bunuasunthon, Ms. Panitporn Laowpanitchakorn, Ms. Li He, Mr. Rentaro Sakamoto, Ms. Wu Chun-Yi, Ms. Riko Akehi, Mr. Ryoto Itani, Mr. Kanta Iwamoto, Ms. Aya Nagura, Ms. Itsuki Miyaguni, Ms. Hong Young Kyoung, Ms. Tomoka Iida, Mr. Kanta Ogura, Ms. Rino Kamada, Ms. Ryo Sekiya, Mr. Takuro Kawamoto, Mr. Tomoya Ushiroda, Mr. Kohei Uno, Ms. Sayaka Oshitani, Ms. Reina Funatomi, Mr. Kakeru Yasumoto. Thanks to their accompany and kind support for both research and daily life.

I would like to acknowledge the financial support from Japan Student Services Organization (JASSO) and Next-Generation program (SPRING JPMJSP2138). And finally, thanks to my family and friends who endured this long process with me, always offer support and love.

June 2024

ZHANG ZHUYING